

Sandstones and Utah's canyon country: Deposition, diagenesis, exhumation, and landscape evolution

**David Loope
Richard Kettler**

Department of Earth & Atmospheric Sciences, University of Nebraska, Lincoln, Nebraska 68588, USA

Kendra Murray*

Department of Geosciences, University of Arizona, Tucson, Arizona 85721, USA

Joel Pederson

Department of Geology, Utah State University, Logan, Utah 84322, USA

Peter Reiners

Department of Geosciences, University of Arizona, Tucson, Arizona 85721, USA

ABSTRACT

South-central Utah's prominent sandstones and deeply dissected landscapes are the focus of this four-day trip, which begins and ends in Grand Junction, Colorado. Studies of the apatite grains in sandstones adjacent to igneous intrusions are revealing new information on the timing and rate of Cenozoic erosion. Iron-oxide-cemented concretions in other rocks record how reduced-iron carbonates and sub-surface microbes interacted when near-surface, oxygenated waters started to flush the reducing, CO₂-rich waters from Colorado Plateau aquifers. New geochronologic techniques that are being applied to the plateau rocks have the potential to expand our knowledge of how diagenetic episodes relate to the evolving topography of this classic geologic setting.

INTRODUCTION

The Colorado Plateau has been the focus of geologic studies since 1869, when a small party led by John Wesley Powell first navigated the canyons of the Green and Colorado Rivers in 1869–1870. Based on the observations and maps made during those early expeditions, Powell championed the importance of uplift and incision to geomorphology, and introduced the concept of base level. His first scientific publication (Powell, 1873)

concerned the main area visited by this field trip, south-central Utah, where Mesozoic and Cenozoic strata rise northward from the Grand Canyon “like a great geographical stairway” (Worster, 2002, p. 311). Two of Powell's protégés did extensive geologic studies in this area. In the middle 1870s, Clarence Dutton and his field crew mapped the geology of 31,000 km² in southern Utah's High Plateaus. He coined the term “isostasy,” and concentrated his studies on erosional landscapes generated by the “Great Denudation.” G.K. Gilbert's thorough study of the Henry

**Current address:* Department of Earth & Environmental Sciences, University of Michigan, Ann Arbor, Michigan 48109-1005, USA.

Mountains went far beyond the coining of the term “laccolith”; he was a process geomorphologist before process geomorphology was cool.

The purposes of this trip are (1) to stimulate discussions of the timing, rates, and drivers of plateau denudation, and (2) to explore the linkage between sandstone exhumation and iron diagenesis. We will visit sites in south-central Utah where research on sandstone deposition and diagenesis is being pursued hand-in-hand with the study of plateau denudation. We have chosen stops that expose participants to great outcrops and vistas, that consist of a variety of geologic processes and materials, and that support these two objectives.

The history of Cenozoic surface uplift and erosion of the Colorado Plateau remains surprisingly enigmatic, despite decades of research along the southwestern margin of the plateau (i.e., the Grand Canyon region) and in the plateau interior (i.e., the Canyonlands region). Diverse tools have been used in recent years to resolve the timing of local and regional erosion patterns and diagenetic mineralization: (1) cosmogenic isotopes; (2) optically stimulated luminescence (OSL); as well as (3) radioisotopic systems used for thermochronology—fission-track dating in zircon and apatite; potassium-argon and argon-argon dating in apatite; uranium-thorium-helium dating in zircon, apatite, and iron oxide; as well as $^4\text{He}/^3\text{He}$ thermochronology. We will visit a site near Mt. Hillers (southern Henry Mountains) where detrital apatite ages were reset by mid-Tertiary igneous activity and therefore record evidence of significant Pliocene–Pleistocene erosion.

Recent progress in paleogroundwater, geomicrobiology, astrobiology, and carbon sequestration has sparked interest in iron-rich concretions, bleached sandstones, and natural CO_2 res-

ervoirs and seeps on the plateau. We will see an example of a CO_2 -charged spring at our first trip stop (Fig. 1). At Crystal Geyser (near Green River, Utah), cool, CO_2 -charged water has been flowing to the surface for at least 400,000 yr. We will examine some of the travertine mounts built along a normal fault.

Thick, cliff-forming eolian sandstones of Jurassic age are widespread on the plateau, and are prominently displayed in Capitol Reef and Zion National Parks, and Grand Staircase–Escalante National Monument. On this trip, we will visit several outcrops of the large-scale cross-bedded Navajo Sandstone, and we will also see prominent cliffs exposing the Wingate and Entrada Formations. Some of the largest sand seas (ergs) known in Earth history accumulated along the western coast of the supercontinent Pangea, and are now recorded by these strata.

The colorful cliffs of the Grand Staircase reflect the diagenetic histories of plateau strata. The now-bleached cross-strata of the White Cliffs (upper Navajo Sandstone) were iron donors to the present-day iron-oxide concretions and bands of the Vermilion Cliffs (lower Navajo). Sandstones of the Triassic Shinarump Member (which form the Chocolate Cliffs, near the Utah-Arizona border; Fig. 1) display intricate patterns of iron-oxide bands and stains. Similar chemical and biological processes operated within the pore spaces of the two formations, but the timing of events was different. The Navajo Sandstone’s iron became mobile long after the desert sands were deeply buried, but, for the Shinarump Member, iron started to move shortly after deposition.

Iron is mobile only in reducing or strongly acidic waters. The Shinarump sands were saturated with reducing water immediately after their deposition, because they lay adjacent to floodplains that were heavily vegetated. Eolian dune fields, however,

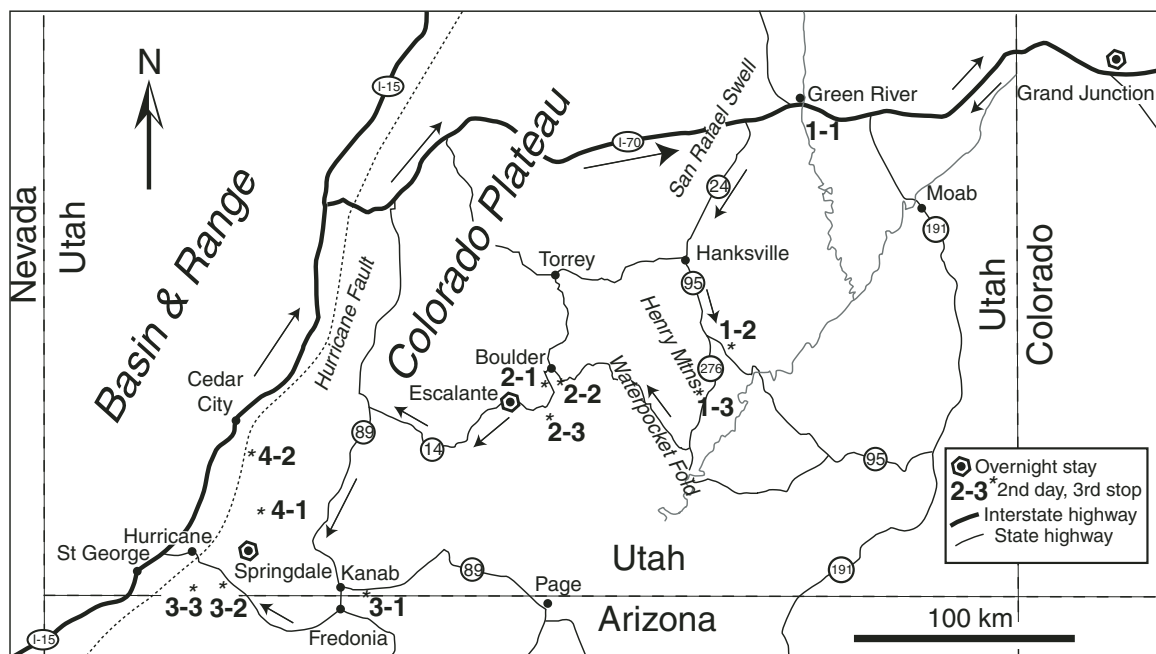


Figure 1. Route for four-day GSA field trip.

support little vegetation, so shallow groundwater in the Navajo desert sand was oxidizing. Shinarump iron was mobile in the Triassic aquifer system, but Navajo iron had to wait more than 100 m.y. to be liberated by deep-sourced, upward-migrating methane. The iron-oxide concretions and bands in both formations, however, formed during the Neogene when precursor, reduced-iron minerals were oxidized by near-surface groundwater as the Colorado Plateau was dissected. The ages, orientations, and distributions of these iron oxides are providing valuable information on the rate and spatial pattern of plateau exhumation.

Field-trip stops will involve walking (up to 5 km), but little strenuous hiking. When the sandstones are dry, footing is good on sloping outcrops. If the outcrops are wet (or, even worse, frozen), avoid the steeper slopes, especially those that support heavy lichen growth. Compared to surrounding parts of the western United States, poisonous snakes in the field area are small, shy, and rare, and spiny plants and stinging and/or biting insects are relatively easy to avoid. We will do our best to provide adequate opportunities for restroom breaks.

GEOLOGIC BACKGROUND

Cenozoic Uplift and Erosion of the Colorado Plateau

The plateau's distinctly and famously intact stratigraphy is largely owed to a lack of deformation during the early Cenozoic Laramide orogeny that transformed the surrounding Interior West (e.g., Spencer, 1996). On the other hand, the episode of lithospheric modification and magmatism (the Oligocene "ignimbrite flareup"), following on the heels of the Laramide, affected the entire Interior West, including the Colorado Plateau (e.g., Humphreys et al., 2003; Schulze et al., 2015). The Henry Mountains laccolith complex (Gilbert, 1877; Hunt et al., 1953) is an example encountered on this trip. More subtle and poorly known is that the plateau experienced relative landscape stability for much of the subsequent middle Cenozoic (e.g., Pederson et al., 2002), although early workers recognized evidence for this episode of "peneplanation" (Davis, 1901). Finally, of great recent interest to researchers, the late Cenozoic has been marked by a change to deep incision of the plateau, including Grand Canyon as we know it, as the Colorado River became integrated to flow into the low Basin and Range province (Lucchitta, 1972; Pederson et al., 2002; Karlstrom et al., 2014). Sources of late Cenozoic, epeirogenic uplift to help drive this erosion remain actively debated (cf. Karlstrom et al., 2008; Pederson et al., 2013a).

Past research tended to lump the entire Colorado Plateau as having one geologic history of uplift and erosion, but this is misleading. In fact, the varying terrain encountered along this field trip across the plateau presents interesting contrasts in Cenozoic landscape evolution, which recent research is starting to resolve. The central Colorado Plateau, at Crystal Geysers and the Henry Mountains for example, has its own distinctively younger story of erosion and landscape evolution (Pederson et al., 2013a; Jochems and Pederson, 2015; Murray et al., 2016). In contrast, the plateau

margin around Zion National Park (explored at the end of this trip), and particularly in the western Grand Canyon area, is the focus of recent scientific controversy because of its complex and long paleo-canyon-cutting history spanning the Cenozoic (cf. Polyak et al., 2008; Wernicke, 2011; Flowers and Farley, 2012; Karlstrom et al., 2014). The plateau edge also has moderately active faulting as well as prospects for some late Cenozoic uplift driven by mantle dynamics (Moucha et al., 2009; van Wijk et al., 2010; Levander et al., 2011).

At the start of this field trip, in the Canyonlands of the central Colorado Plateau, we explore the late Cenozoic timing of the onset of significant erosion, as well as the spatial and temporal patterns in this exhumation, which has removed up to 3 km of overlying strata (Nuccio and Condon, 1996; Lazear et al., 2013; Murray et al., 2016). These patterns of erosion have been hypothetically linked to varying bedrock strength across the plateau, the distinctive weathering and erosion of sandstones, and to the isostatic feedback between rock uplift and exhumation (Pederson et al., 2013a; Bursztyn et al., 2015).

The Paleozoic and Mesozoic sandstones in the Canyonlands region contain detrital apatite grains with diverse pre-depositional thermal histories, variable crystal chemistries, and a post-depositional history residing at apatite He partial retention temperatures (40–80 °C; ~1–4 km depth). These factors can make resolving the most recent cooling and exhumation of these rocks using low-temperature thermochronology difficult (Carter and Gallagher, 2004; Gautheron et al., 2013; Fox and Shuster, 2014). Fortunately, in the Henry Mountains, these sandstones have a thermal history that was punctuated ca. 28–25.5 Ma by the emplacement of the laccoliths, which overprinted their convoluted thermal history and primed them to document only the post-Oligocene history of rock cooling (Fig. 2).

Deposition and Diagenesis of the Navajo Sandstone

The Navajo-Nugget-Aztec Sandstone represents the preserved remains of a giant, Early Jurassic sand sea. These formations now cover broad portions of Wyoming, Utah, Arizona, and Nevada (Kocurek and Dott, 1983). Studies based on the detrital zircons that accompany this huge volume of quartz sand have shown that westward-flowing rivers draining the slopes of the Appalachians delivered billion-year-old sand to an area just north of the erg (Dickinson and Gehrels, 2003; Rahl et al., 2003). Winds out of the north (recorded by the dip direction of the cross-strata) delivered this sand to the Navajo and the Entrada ergs. The same systems delivered sand for the thick late Paleozoic eolian sandstones (Coconino, Cedar Mesa, Weber, White Rim) of the Colorado Plateau.

Thick sets of cross-strata composed of fine to medium sand are highly suggestive of eolian dune deposits, but the most diagnostic indicators are the inverse-graded, wind-ripple laminations that make up a large percentage of the Navajo Sandstone (Hunter, 1977, 1981). Grain flows (dry avalanche deposits) are thicker (up to 15 cm) and steeper than the wind-ripple deposits. After compaction

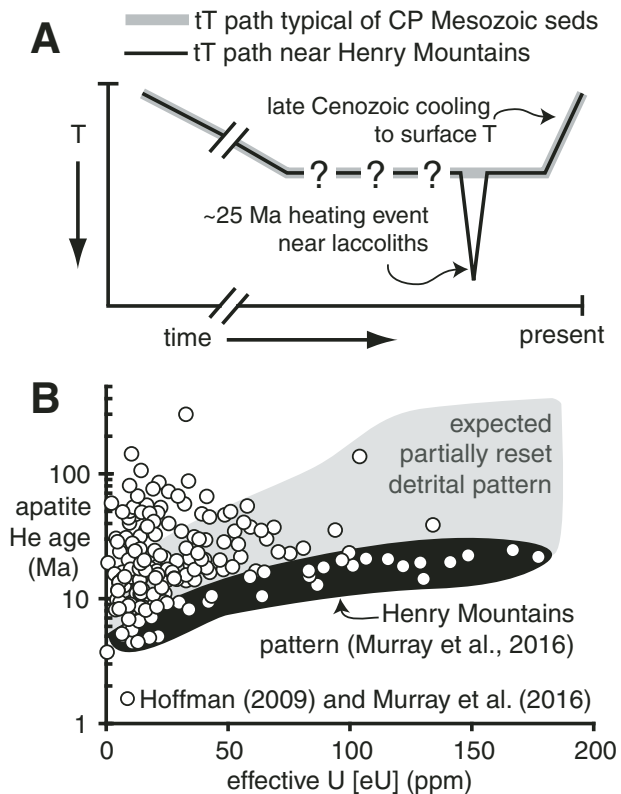


Figure 2. (A) Schematic temperature-time paths of the Paleozoic and Mesozoic sedimentary rocks in the Canyonlands region of the Colorado Plateau, and (B) the corresponding apatite He age versus effective U [eU] trends generated by these thermal histories (gray fields) compared to single-grain apatite He results from across the central Colorado Plateau (Hoffman, 2009; Murray et al., 2016). Heating of these rocks ca. 28–25 Ma in the thermal aureole of the Henry Mountains largely resets the enigmatic He age variability characteristic of the Canyonlands region's sandstones and provides a tight thermal constraint useful for robust thermal history modeling of the positive-slope age-[eU] trend.

from their original 32°, most grain flows now dip ~25°. Upon deposition, they were much looser packed than wind-ripple deposits, and therefore more vulnerable to soft-sediment deformation. Widely attributed to seismic events, this deformation generated large-scale folds and faults, and extensive brecciation (Doe and Dott, 1980; Bryant and Miall, 2010; Loope et al., 2013; Chan and Bruhn, 2014). Horowitz (1982) made a strong case that preferential liquefaction below interdunes can cause adjacent dunes to collapse, generating strong lateral compression.

The ubiquitous cross-bedded dune deposits in the Navajo Sandstone demonstrate, however, that shallow groundwater was well oxygenated and that little organic matter was preserved in the sedimentary environment. The “bleached” upper Navajo that forms the White Cliffs of the Grand Staircase records a late-diagenetic episode in which reducing fluids moved through the formation, dissolving the iron-oxide coatings on sand grains and

mobilizing ferrous iron (Beitler et al., 2003, 2005). The iron liberated by the reducing fluids later precipitated as iron-rich concretions in the lower Navajo Sandstone (Beitler et al., 2005).

The iron-oxide-cemented concretions have been interpreted as: (1) *de novo* precipitates produced by the mixing of reducing, iron-bearing fluids with oxygen-bearing meteoric water (Beitler et al., 2005; M.A. Chan et al., 2011), or as (2) the altered remains of precursor concretions cemented by siderite (FeCO_3 ; Loope et al., 2010, 2011). The presence of iron-oxide rhombs in many of these concretions is the strongest outcrop-scale evidence for the precursor hypothesis. Rhombic siderite is a common early-diagenetic cement in fluvial sand bodies that underlie marshy floodplain deposits (Loope et al., 2012; Kettler et al., 2015; Burgess et al., 2016). The central areas of many Navajo concretions contain rhombic, iron-oxide pseudomorphs similar to those preserved in channel sandstones of the Dakota Formation of eastern Nebraska, and to those in the Shinarump Member of the Chinle Formation. Loope et al. (2010) and Loope and Kettler (2015) argued that iron-rich carbonates precipitated in the Navajo Sandstone when dense, reducing waters carrying ferrous iron and dissolved CO_2 moved downward from structural highs, thereby explaining the lower stratigraphic position of the iron-rich concretions relative to the bleached, donor beds of the upper Navajo. In addition to the iron-oxide concretions, abundant and well-preserved ferrous-calcite concretions are also present in the lower Navajo Sandstone.

We interpret the concretions as the products of iron-oxidizing microbes that used siderite as a source of both energy and carbon. The microbes of interest are microaerophiles. They do not flourish in waters with high oxygen content, nor in strongly acidic waters where pyrite is being oxidized. At near-neutral pH, and low oxygen concentrations, however, they can metabolize ferrous iron 60× faster than the abiotic oxidation rate (Konhauser et al., 2002). The iron-oxide-cemented bands and rinds in the Navajo Sandstone were produced by microbial biofilms that established themselves at redox boundaries. As siderite concretions or disseminated siderite crystals dissolved, ferrous iron diffused to the redox boundary and ferric oxide minerals precipitated. The precipitation of ferric oxide minerals generated acid that then diffused toward the siderite, accelerating its dissolution.

The oxides take the form of the redox boundaries, and they can be grouped in three different “families” by shape: rinds, scallops, and columns (Fig. 3). The thicknesses of the structures depend on how much ferrous iron diffused to the microbial biofilm before the redox boundary shifted.

CO₂ Reservoirs, Bleached Sandstones, and Reducing Fluids

Using satellite imagery and field-based spectral reflectance measurements, Beitler et al. (2003, 2005) showed that the Navajo Sandstone is iron depleted across many Laramide structural highs. They hypothesized that these bleached sandstones may mark the positions of “exhumed hydrocarbon giants”—large

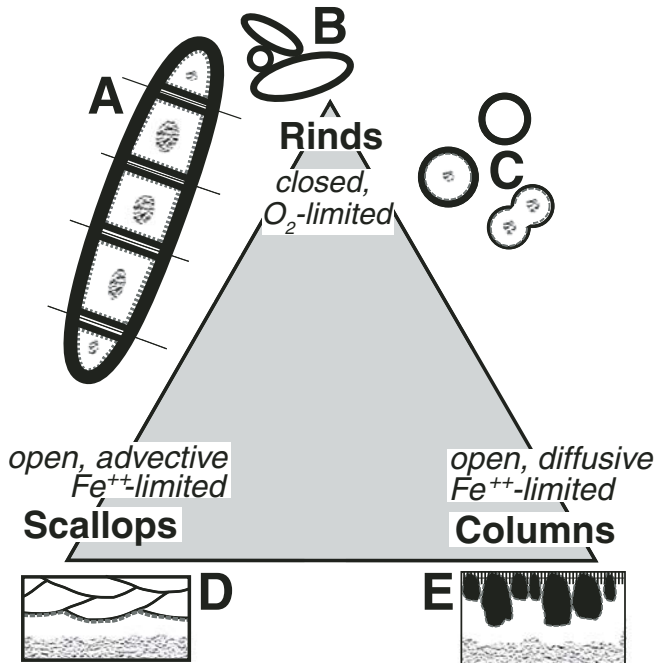


Figure 3. Three families of iron-oxide-cemented structures, the conditions needed for their development, and five examples. Siderite was the local source of iron for all the iron-oxide cement shown. Black lines are iron-oxide-cemented sandstone; white spaces are iron-poor sandstone; stippled areas are sandstone with disseminated siderite cement crystals. Thin, straight lines are fractures. Dashed lines show positions of active biofilms. Microbes remained active until all adjacent siderite was consumed. (A) Boxworks developed from oxidation of meter-scale siderite concretions that were oxidized after jointing (Loope and Kettler, 2015); (B) sideritic mud balls oxidized after fluvial transport (Loope et al., 2012); (C) marbles—small spheroids with iron-oxide rinds developed during oxidation of siderite concretions of the same size and shape (Weber et al., 2012); (D) wonderstone (Kettler et al., 2015); and (E) columnar structures resembling stromatolites. From Loope et al. (2016).

hydrocarbon reservoirs that have been breached by erosion. No bitumen, however, has been reported from bleached Navajo Sandstone, and only a very small quantity of bitumen is present in the Entrada Sandstone (at one site). The $\delta^{13}\text{C}$ values of carbonates associated with the bleached rocks indicate that at least a portion of the carbon was derived from organic sources (Fig. 4). This evidence, combined with the widespread surviving and altered carbonate concretions, agrees with the suggestion of Haszeldine et al. (2005) that the bleaching was accomplished via large volumes of carbon dioxide and a lesser amount of methane.

Two linked, density-driven flow systems may have operated to bleach the sandstone and to transport sufficient iron to precipitate iron-carbonate concretions over a large portion of southern Utah: (1) buoyant up-dip flow of methane and supercritical carbon dioxide; and (2) convective flow driven by the enhanced density of waters carrying aqueous CO₂ in contact with over-

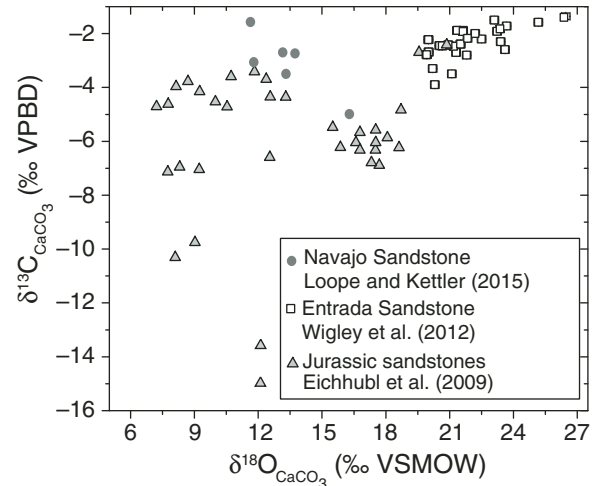


Figure 4. Plot of carbon and oxygen isotopes for calcite cements and concretions from southern Utah and comparison with values from other sandstones in the region. Triangles mark values from Chan et al. (2000), Eichhubl et al. (2009), and Garden et al. (2001). Modified from Wigley et al. (2012) and Loope and Kettler (2015). VPDB—Vienna Pee Dee belemnite; VSMOW—Vienna standard mean ocean water.

lying, migrating or trapped supercritical CO₂ (Fig. 5). Dissolution can yield a solution that is ~5 wt% CO₂. Bickle (2009) noted that if the reservoir has high permeability, a 50-m-thick layer of CO₂ can be dissolved in 10 yr. Upslope migration continually exposes migrating CO₂ to unsaturated waters, making dissolution more efficient; descent of the denser, CO₂-charged waters can arrest the upslope flow of the buoyant fluid (MacMinn and Juanes, 2013; Fig. 5). The great extent and relatively uniform thickness of the bleached rock on the Colorado Plateau (e.g., the White Cliffs from Springdale to Page; Fig. 1) reflect the interaction of these two flow systems. The low northward dip of the Navajo Sandstone along the east-west-oriented White Cliffs of southwestern Utah suggests that CO₂ migrated southward toward a broad, now eroded structural high. The abundance of concretions along the east flank of the Kaibab upwarp indicates that CO₂ very likely accumulated along the crest of that structure. Rather than developing only within or immediately below giant CO₂ reservoirs, however, a large proportion of the bleached rocks and carbonate concretions most likely developed along gently sloping flow paths along which the CO₂ and methane never reached a structural trap (the dense water descended before reaching a trap or the ancient land surface; Fig. 5).

Hydrodynamic flow may have also played a role in the bleaching and emplacement of concretions. The positions of the Escalante anticline and the Aquarius Plateau were suitable for hydrodynamic flow through the Navajo Sandstone during portions of the middle and late Cenozoic (Loope et al., 2010). A sister anticline just west of the Escalante structure (the Upper Valley anticline) presently has hydrodynamic flow from the Aquarius Plateau (Allin, 1993).

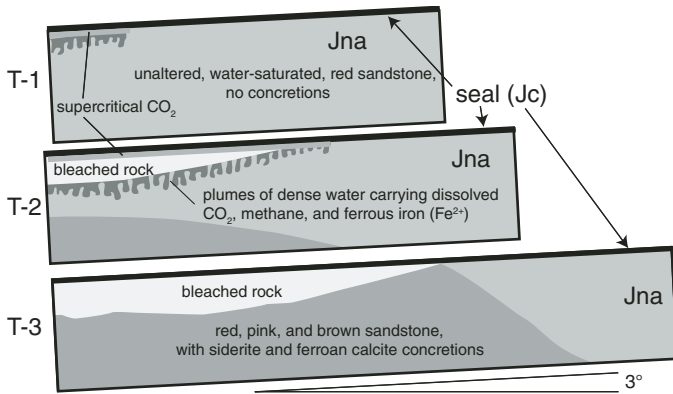


Figure 5. Model for bleaching of upper Navajo Sandstone and precipitation of ferrous carbonate concretions in the middle Navajo. T-1: Moving up dip, just below the sealing Carmel Formation, buoyant, supercritical carbon dioxide and a small quantity of methane starts to accumulate in the upper Navajo Sandstone. Dissolution of CO_2 into underlying water begins, increasing the density of the aqueous solution (Kettler et al., 2011). T-2: Supercritical carbon dioxide in contact with underlying formation water continues to move up dip and to dissolve, whereas the denser fluid moves downward as finger flow. Methane reduces hematite on the rims of sand grains, releasing ferrous iron into solution and bleaching the rock. The descending water transports ferrous iron and remaining methane downward. T-3: Carbon dioxide is depleted, and downward flow has ceased. Siderite and ferroan calcite have precipitated in the middle Navajo Sandstone (perhaps facilitated by localized degassing of carbon dioxide). The up-dip extent of bleached rock marks the limit of CO_2 migration, providing a possible explanation for the presence of unbleached sandstone in northernmost Zion National Park (noted by Nielsen et al., 2009). Final thickness of bleached zone reflects quantity of methane available for ferric-iron reduction during descent of plumes. Modified from MacMinn and Juanes (2013, fig. 1) and Loope and Kettler (2015, fig. 11). Jna—Jurassic Navajo Sandstone; Jc—Jurassic Carmel Formation.

At least 11 Colorado Plateau anticlines presently contain large volumes of carbon dioxide (Haszeldine et al., 2005). Gilfillan et al. (2008; Fig. 6) studied the noble gas geochemistry of five natural CO_2 reservoirs from the Colorado Plateau and Rocky Mountain provinces and concluded that the dominant sources of all fields were magmatic. In the transition zone to the Basin and Range province, explosive igneous activity was widespread on the plateau during the middle and late Cenozoic. The lavas exposed in the northern part of our study area (Fig. 6) are part of the Marysvale volcanic field, one of the largest in the western United States. Most calc-alkaline magmatic activity occurred during the Oligocene and Miocene (32–22 Ma), and the less voluminous bimodal basalts and rhyolites were emplaced as recently as the Holocene (Rowley et al., 2002). The Marysvale field is at the eastern edge of a caldera complex that was centered on what is now the Basin and Range province. Some of the springs located along faults in the Grand Canyon issue mantle-derived CO_2 and helium (Crossey et al., 2006, 2009). Work on springs and travertines shows that although some portions of these gases reflect ongoing processes in the

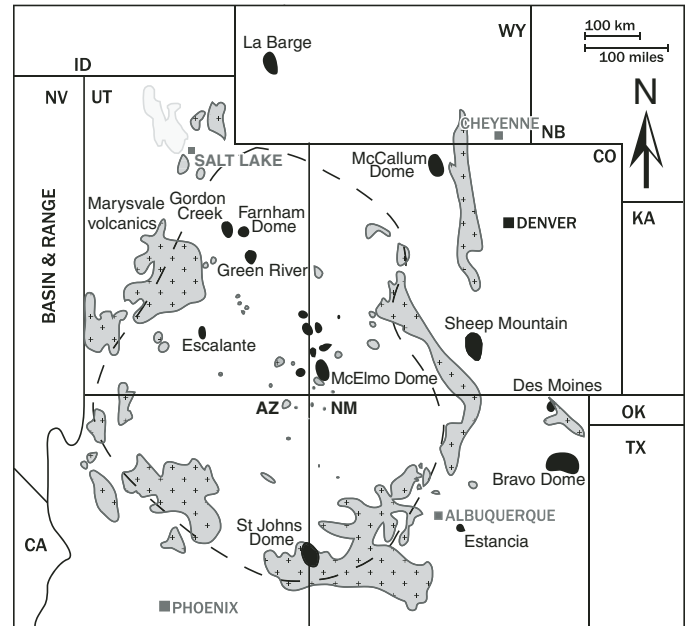


Figure 6. Cenozoic igneous rocks (gray) and natural CO_2 reservoirs (black). Dashed line marks the perimeter of the Colorado Plateau. Redrawn from Allis et al. (2001), Gilfillan et al. (2008), and Kampman et al. (2014). AZ—Arizona; CA—California; CO—Colorado; ID—Idaho; KA—Kansas; NB—Nebraska; NM—New Mexico; NV—Nevada; OK—Oklahoma; TX—Texas; UT—Utah; WY—Wyoming.

asthenosphere, another strong component was released during the Oligocene (Crossey et al., 2009).

At Crystal Geyser near the town of Green River, Utah (Stop 1-1; Fig. 1), carbon dioxide has been escaping for more than 100,000 yr from a faulted reservoir in the Navajo Sandstone (Shipton et al., 2005; Heath et al., 2009; Burnside et al., 2013). Wigley et al. (2012) and Kampman et al. (2014) showed that the escaping fluid has extensively bleached the overlying Jurassic Entrada Sandstone and that ferroan carbonates are forming at the reaction front between bleached and unbleached sandstone.

Deposition and Diagenesis of the Shinarump Member of the Chinle Formation

The Shinarump Member is a thin, cliff-forming sandstone at the base of the Upper Triassic Chinle Formation. This unit overlies an erosional unconformity cut into the Moenkopi Formation. Detrital zircons and paleocurrents indicate the Chinle stream system flowed northwestward from central Texas toward central Nevada. Due to low accommodation, little mudstone was preserved between the fining-up channel sandstone bodies deposited by sinuous streams. Distinctive mud balls are common as channel lags at the bases of these sand bodies: thick, iron-oxide rinds cement their perimeters. Such rinds indicate that early-diagenetic siderite had formed in the floodplain mud before mud balls were eroded from stream banks (Loope et al., 2012; Burgess et al.,

2016). Rhomb-shaped, iron-oxide cements are abundant in Shinarump sandstones. These are pseudomorphs after siderite and indicate that recharging, methanic groundwater that had moved downward through floodplain muds introduced ferrous iron into the underlying channel sands, where it precipitated as siderite. Instead of forming pseudomorphs, however, much of the siderite that precipitated in the channel sands was, during late diagenesis, metabolized by iron-oxidizing microbes and precipitated as complex bands of iron oxide that is known (and marketed) in southern Utah as “wonderstone” (Kettler et al., 2015). The wonderstone and the rinds on the transported mud balls postdate lithification of the Shinarump Member, and developed during Neogene exhumation of the Triassic strata. The preserved microbes (which resemble modern *Gallionella*) resided in shallow groundwater charged with a small amount of oxygen.

Geochronologic Tools for Understanding Timing and Rates of Plateau Exhumation and Diagenetic Mineralization

Radioisotopic dating techniques useful for understanding thermal and fluid flow histories of rocks in the Colorado Plateau include the fission-track, (U-Th)/He dating in apatite and zircon grains, and $^{40}\text{Ar}/^{39}\text{Ar}$ dating of diagenetic cements and veins. The fission-track system relies on spontaneous fission of ^{238}U that is present in trace concentrations (typically tens to thousands of ppm) in minerals. Fission creates damage tracks whose density can be combined with U concentrations and the fission decay constant for ^{238}U to yield a fission-track age of the mineral. Similarly, radiogenic ^4He is produced by ^{238}U , ^{235}U , and ^{232}Th (and to a much lesser degree by ^{147}Sm), and the relative amounts of these parent and daughter nuclides can be combined with the appropriate decay constants to yield (U-Th)/He ages. As both fission tracks and ^4He anneal away or diffuse out of crystals if temperatures are sufficiently high, these techniques typically reflect something about the cooling history of their host rock, rather than necessarily their formation ages. In many cases, the ages can be considered to represent the time elapsed since a sample cooled below a “closure temperature,” which is roughly 50–60 °C for apatite and 170–190 °C for zircon. Since these temperatures typically correspond to depths below the Earth's surface of roughly 2–3 km or 7–9 km, respectively, they can be used to estimate the timing and rate of exhumation of rocks through these depths, which in this region is driven predominantly by erosion.

These techniques, as well as the $^{40}\text{Ar}/^{39}\text{Ar}$ system, can also be used in some cases to understand the formation and thermal histories of secondary and diagenetic minerals in sandstones. Chan et al. (2000) showed that Mn oxides in the Navajo Sandstone near Moab had complex $^{40}\text{Ar}/^{39}\text{Ar}$ age spectra that they interpreted as recording formation ca. 25–20 Ma. However, Garcia and Reiners (2015) found a $^{40}\text{Ar}/^{39}\text{Ar}$ plateau on a related Mn-oxide vein with a relatively precise age of 3.60 ± 0.08 Ma and $^4\text{He}/^3\text{He}$ -(U-Th)/He thermochronologic results also pointing toward formation at 3.6 Ma. Reiners et al. (2014) also measured (U-Th)/He ages of goethite and hematite cements and veins in

the Navajo Sandstone in southern Utah. Although some samples yielded apparent Miocene ages, most of the samples appear to be Pliocene–Pleistocene, though some of these young ages may reflect late addition of U and Th from shallow groundwater.

ROAD LOG

■ DAY 1

Directions to the first stop. We will leave Grand Junction via I-70 west and drive 100 miles (mi) to Green River, Utah. Take Exit 164 off of I-70 (East Main Street), drive south on the overpass and turn left (east) at the “T” on New Area 51 Road. After ~2 mi, where this road intersects the Crystal Geysers Road, turn right. After winding up a gentle dip-slope of Jurassic Morrison Formation, turn west to parallel the Little Grand Wash fault. Follow the valley of Little Grand Wash for ~5 mi. After a final right turn before crossing the wash, the road ends along the east bank of the Green River, where Crystal Geysers issues to the surface. We will park, stroll around the geysers area, and then gather to tromp east along the trace of the fault and onto a Pleistocene terrace underlain by interfingering travertine and gravel. Walk west along this finger-shaped remnant to an overview of the Crystal Geysers area.

Stop 1-1: Crystal Geysers (38° 56.299' N, 110° 8.128' W)

An exception to the general lack of Cenozoic structural deformation in the Colorado Plateau is the episodic salt tectonics linked to unloading of Pennsylvanian evaporite deposits of the ancestral Paradox basin. In the cases of the Grabens district of Canyonlands in southeastern Utah and the Onion Creek diapir and Professor Valley area in east-central Utah, it has been established that deformation has been ongoing over the Pleistocene (Colman, 1983; Huntoon, 1988; Furuya et al., 2007; Jochems and Pederson, 2015). Here at Crystal Geysers, the Little Grand Wash fault crossing the Green River, as well as the Salt Wash (aka Ten-Mile) graben faults downstream, faulting is potentially active based upon initial mapping of travertine and fault relations (Shipton et al., 2004). These faults have acted as pathways for fluid flow, resulting in a set of abandoned and modern spring-travertine mounds focused along the fault traces (Shipton et al., 2004; Dockrill and Shipton, 2010; Kampman et al., 2012). The south-dipping Little Grand Wash normal fault has an arcuate surface trace of 61 km and a total vertical separation in the study area of 180–210 m (Fig. 7A; Dockrill and Shipton, 2010). Like the other NW-SE-oriented normal faults of the region, the Little Grand Wash fault is thought to sole in the Paradox Formation evaporites at depth, though a deeper link to basement structures is also possible (Black and Hecker, 1999; Trudgill, 2011).

The Crystal Geysers study area lies along the Green River, which exits Desolation-Gray Canyon through the Book Cliffs upstream and crosses low-relief, arid badlands underlain by the upper Cretaceous Mancos Shale before entering Labyrinth

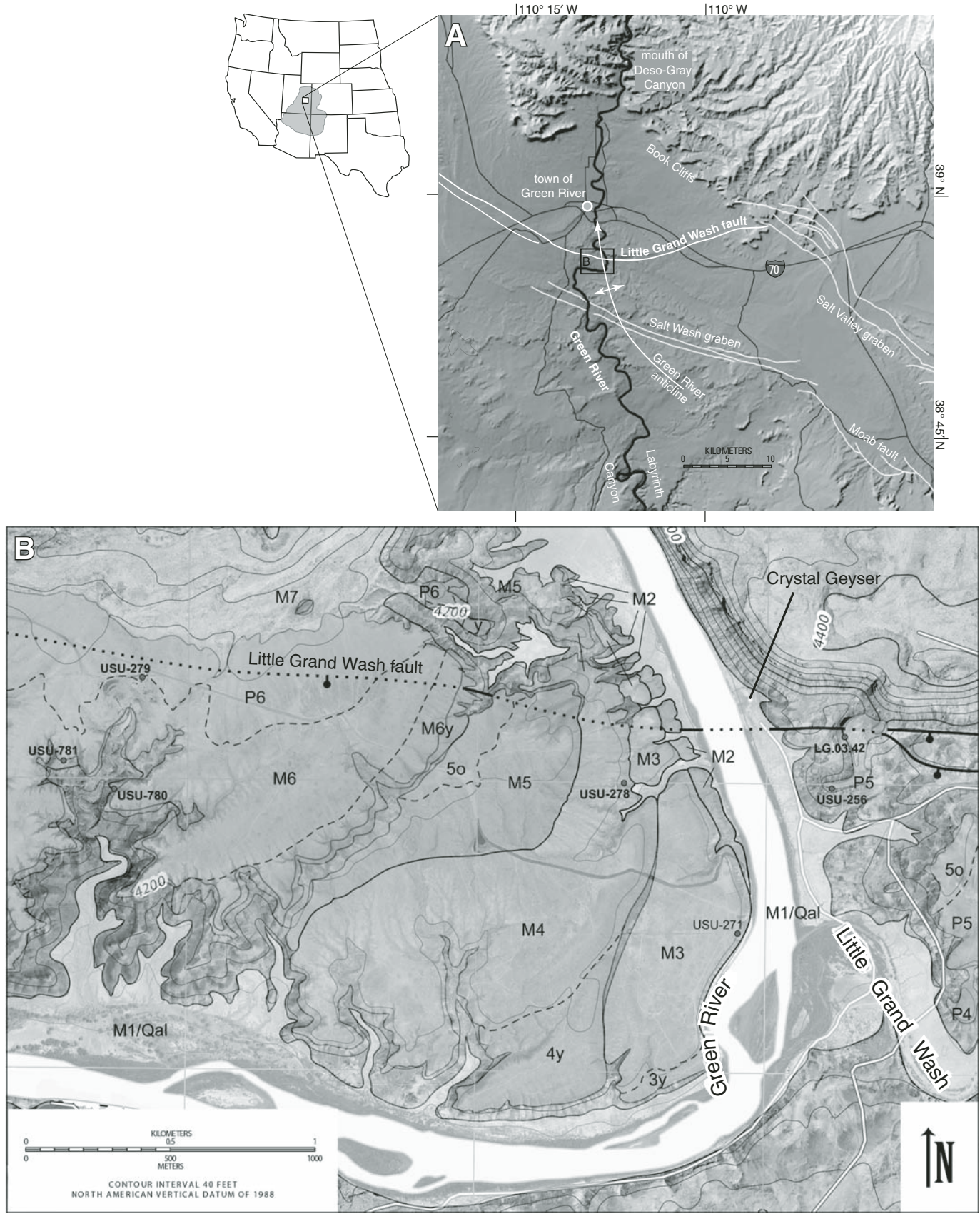


Figure 7.

Figure 7. (A) Location of the Crystal Geyser study area, Stop 1-1, in the north-central Colorado Plateau, in the badlands downstream of the mouth of Desolation–Gray Canyon and upstream of Labyrinth Canyon. (B) Mapped fluvial terrace deposits and chronology sample locations near where the Green River crosses the Little Grand Wash fault. Terrace deposits are identified as M7 to M1 for “mainstem” Green River deposits from oldest to youngest, P6 and P5 are local “piedmont” deposits graded to mainstem terraces, and “y” and “o” are modifiers added where multiple, younger or older, terrace landforms are set upon the same deposit. Samples for numerical ages were taken at locations marked with USU-# for optically stimulated luminescence and LG.03.42 for U-series. Modified from Pederson et al. (2013b).

Canyon (Fig. 7A). As the river approaches the Little Grand Wash normal fault, the lower Cretaceous Cedar Mountain and the Jurassic Morrison and Summerville Formations rise in the footwall. Where the river crosses into the hanging wall, the Mancos Shale is brought to river level again, the valley broadens, and there is preserved a suite of seven gravelly strath terraces in an interior bend of the river (Fig. 7B).

Crystal Geyser itself is a periodic, CO₂-charged geyser created by an oil exploration well drilled in AD 1935 (McKnight, 1940). Travertine precipitates out of the CO₂-saturated water exiting the well, and there is a 113-k.y.-long record of fracture-fill and travertine formation along the central part of the fault trace (Burnside et al., 2013). Previous work at the site has focused on the Little Grand Wash fault as a conduit for CO₂ and water; it has been interpreted to record pulses of CO₂ leakage potentially linked to climate changes (Kampman et al., 2012). Ancient travertine deposits along the fault are found up to 37 m above those presently forming at Crystal Geyser, and usually form resistant caps to erosional remnants. The travertine body we will explore just east of the Green River issues from one such remnant mound, which has been dated by uranium-series methods. This travertine stratigraphically underlies and interfingers with local piedmont alluvium in a complex terrace remnant graded to a past level of the main-stem Green River (P5 in Fig. 7B).

Chronostratigraphy at Crystal Geyser

Full methods and results documenting the stratigraphy and chronology of river terraces are found in Pederson et al. (2013b), including for OSL and U-series dating. Seven distinct main-stem (M1–M7) Green River strath-terrace deposits were identified in the Crystal Geyser map area (Fig. 7B), with some additional fill-cut terrace levels beveled upon them. The most prominent Pleistocene terraces range from 12 m (M2) to 56 m (M6) in height above the modern channel edge, whereas the M1 is a series of finer-grained Holocene deposits of the river floodplain and travertine near Crystal Geyser with dates ranging from ~9–5 ka (Fig. 8; Burnside et al., 2013). Pleistocene terrace deposits M2–M7 have well-developed and exposed planar straths, and are capped by up to 10 m of cobbly alluvium where fully preserved. Luminescence age results provide stratigraphically coherent age estimates for deposition of the M6, the capping P6 (“piedmont-6”) and P5, and the inset M4 and M3 deposits. When combined with the U-series results from the basal P6/5 deposit at this stop, it is evident that the upper terraces that dominate the local landscape represent a complex episode of river planation and gravel deposition from ~115–85 ka (Fig. 8).

The age and surveyed geometry of fluvial terraces can be used to reconstruct the episodic history of river planation and then pulses of incision. The overall bedrock incision rate, integrated over the length of the climate-driven variations recorded here at Crystal Geyser, is ~450 m/m.y. This result for the Green River is similar to other surprisingly rapid trunk-river incision rates calculated in the central Colorado Plateau over the late Pleistocene, and it contrasts with well-constrained, slower incision rates in Grand Canyon farther downstream (Pederson et al., 2013a).

Although the Little Grand Wash fault is well expressed in the landscape by this escarpment, mapping reveals no evidence for scarps along the actual fault trace running along the toe of this embayed ridge. Field relations between the fault plane and the strath terraces of the study area provide more direct evidence that there has been no measurable slip on the Little Grand Wash fault over the past ~100 k.y. The most visible example is the undeformed basal strath of the M6y terrace overlying the trace of the

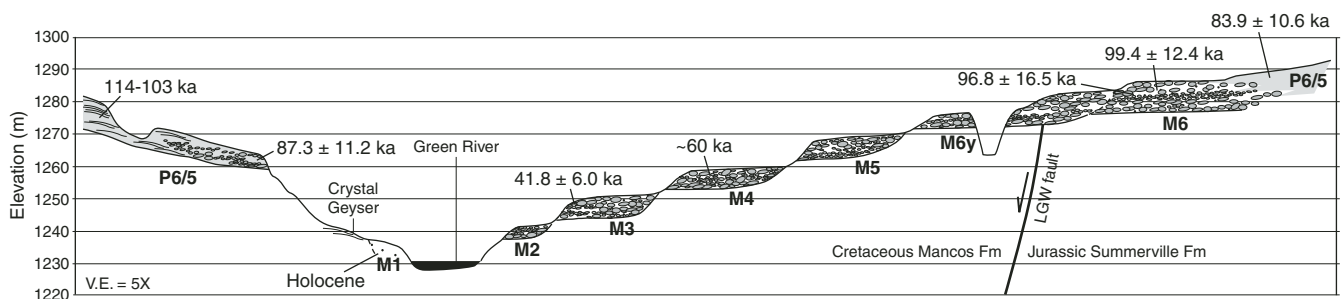


Figure 8. Cross-sectional profile of the terrace stratigraphy at Crystal Geyser, looking downstream, with age results from OSL and U-series dating. **M** denotes mainstem Green River terrace deposits, **P** denotes deposits of local-piedmont systems graded to mainstem terraces. LGW—Little Grand Wash. From Pederson et al. (2013b).

fault exposed in a gully drainage (Fig. 9), thus there has been no surface rupture of the fault over the past ~100 k.y.

Faulting and Deformation in the Central Colorado Plateau

Despite the new information here at Crystal Geyser, constraints on the timing of slip on the Little Grand Wash fault are limited—it was active sometime before 100 ka, and it offsets Late Cretaceous strata. Dockrill's (2006) analysis of local boreholes indicates no resolvable thickness changes across the fault from the Permian to the Cretaceous, and he therefore suggested that the fault initiated during the Laramide. Supporting this, a proportion of slip on the Moab fault nearby to the east has been dated to the early Tertiary (Pevear et al., 1997; Solum et al., 2005).

Any post-Laramide slip on the Little Grand Wash and nearby Salt Wash graben faults may relate to the overall SW-NE extensional state of stress in the central Colorado Plateau (Wong and Humphrey, 1989). In fact, ~100 km to the southwest of Crystal Geyser in the east-central plateau are exhumed mafic dikes dated to 4 Ma by K-Ar methods (Delaney and Gartner, 1997). These have a similar average NW-SE orientation as the normal faults of the region. Linking to the next stops on this field trip, Pederson et al. (2013b) note that this Pliocene component of extension and potential faulting in the region coincides with the start of rapid erosional unloading in the central plateau (Murray et al., 2016). They suggest that the domal or arching pattern of isostatic rebound from the broad-wavelength erosional unloading (Lazear et al., 2013; Pederson et al., 2013a) may have enhanced extension, resulting in movement along structures such as the Little Grand Wash fault and Salt Wash graben.

In regard to recent deformation, the evidence that the Little Grand Wash fault has been inactive over the late Quaternary contrasts with other structures across the ancestral Paradox basin. The hypothetical driver for the recent salt tectonics elsewhere is, in fact, focused canyon incision by the Colorado River system.

This may inspire both deformation from differential unloading of mass above the shallow salt bodies and dissolution and removal of Pennsylvanian salt by groundwater entering the river system, causing graben subsidence (Colman, 1983; Huntton, 1988; Gutiérrez, 2004; Trudgill, 2011; Jochems and Pederson, 2015). Yet, here at Crystal Geyser, these drivers of salt tectonics are not present because the Paradox Formation evaporites are stratigraphically >1.5 km below the land surface, and this is a broad, low-relief landscape instead of a canyon.

Regional Patterns of River Incision

The river incision rate of 450 m/m.y. at Crystal Geyser during the late Quaternary is consistent with the recently recognized bull's-eye pattern of rapid incision in the central Colorado Plateau (Pederson et al., 2013a). The base-level fall required to drive this fast incision of the central plateau must come from a combination of debated sources of rock uplift and Colorado River drainage integration itself. Pederson et al. (2013a) argue that this bull's-eye pattern is inconsistent with recently proposed mantle-driven uplift at the SW flank of the plateau and associated downward tilting of the central and NE plateau (Moucha et al., 2009; van Wijk et al., 2010; Levander et al., 2011), and instead suggest it reflects the feedback between erosional exhumation and flexural-isostatic rebound as mentioned above. This feedback of erosion and rock uplift may drive enhanced erosion in the central plateau as well as extension and salt tectonics, but it was ultimately initiated by the 5–6 Ma integration and base-level fall of the Colorado River propagating upstream from the plateau edge west of Grand Canyon (e.g., Pederson and Tressler, 2012).

Rapid incision in the very broad landscape around Crystal Geyser may seem contrary to expectations at first, because of the common association between steep rivers, high canyon relief, and rapid incision. At Crystal Geyser, the rapidly incising Green River has a relatively low gradient and low-energy expenditure

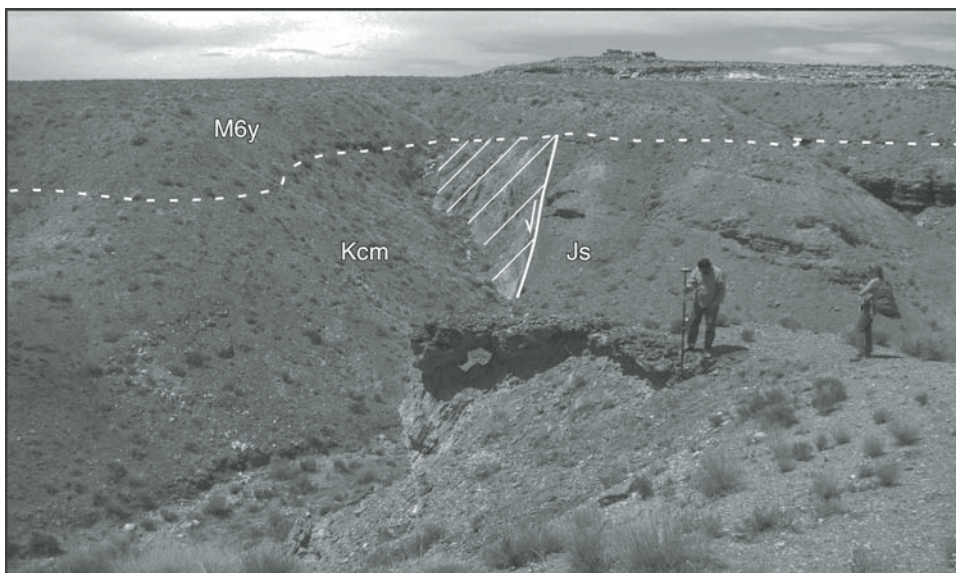


Figure 9. Photograph looking west across a gully drainage into the trace of the Little Grand Wash normal fault. Cretaceous Cedar Mountain Formation (Kcm) offset against the Jurassic Summerville Formation (Js) in the footwall (hachures denote zone of fault deformation). The undeformed strath of the M6y terrace cross-cuts the fault zone, indicating no measurable surface rupture over the past ~100 k.y. From Pederson et al. (2013b).

(Fig. 10), and the entire lengths of Labyrinth and Stillwater canyons just downstream lack any named rapids. Below Cataract Canyon, the Colorado River is likewise low in gradient, yet it has high incision rates like that at Crystal Geyser (Fig. 10; Pederson et al., 2013a). These low-energy, central plateau reaches coincide with a sequence of Jurassic and Cretaceous sandstones and shales at river level, which are of low strength and that provide little coarse bed material to the channel (Bursztyn et al., 2015). Nevertheless, abundant tools for river incision do exist, as is evident from the gravel-clast types of the terrace alluvium in the study area. Hard tools on soft rock accomplish significant incision, as well as lateral planation, forming prominent strath terraces (e.g., Montgomery, 2004; Johnson et al., 2009). The Green River here at Crystal Geyser is representative of the conditions across the central Colorado Plateau, where mechanically weaker Mesozoic rock is eroding rapidly and creating a positive feedback of isostatic rebound, while controlling topography and creating a “deceptively” broad landscape (Bursztyn et al., 2015).

Directions to next stop. We will now drive ~85 mi to our next geologic stop. From Green River, we go west on I-70, and, just before entering the San Rafael swell, we turn southward on Utah 24. We turn south on Utah 95 at Hanksville—the view to the west is of the Henry Mountains and of fluvial terraces composed of diorite porphyry cobbles. Stop 1-2 is ~1.5 mi beyond the turnoff for Utah 276. Lunch break will likely follow this stop.

Stop 1-2: Navajo Sandstone: Dunes and Pond Deposits at North Wash (38° 1.237' N, 110° 32.793' W)

The Navajo Sandstone is well exposed along North Wash; for this short stop, we will focus on physical and biogenic sedimentary structures and on the thin limestones (Fig. 11) that are interstratified with the eolian cross-beds. Wind-ripple laminae (Hunter, 1977) comprise the bulk of the cross-strata. Grain flows (dry avalanches) are also present here, but are commonly contorted. Large-scale, soft-sediment deformation (likely produced by seismic shocks) is visible at several stratigraphic intervals.

Liquefaction requires water-saturated sediment at shallow depth; the presence of the carbonate lenses here is good evidence that the water table was near or above the land surface in broad parts of interdunal areas. Contorted bedding requires not only liquefaction, but also a driving force (Owen, 1996). In a dune field, liquefaction may occur only below interdunes; the vertical stress beneath large dunes is likely to suppress or prevent liquefaction (Horowitz, 1982). Slumping of dunes toward the liquefied sand below the interdunes may have been the driving force for the large-scale folds visible in these outcrops.

The carbonate lenses are widespread, but are most abundant in the lower Navajo Sandstone in eastern and south-central Utah. Large-diameter tree stumps (Parrish and Falcon-Lang, 2007), dinosaur tracks, invertebrate burrows (Riese et al., 2011), and giant stromatolites (Eisenberg, 2003) indicate that the carbonates

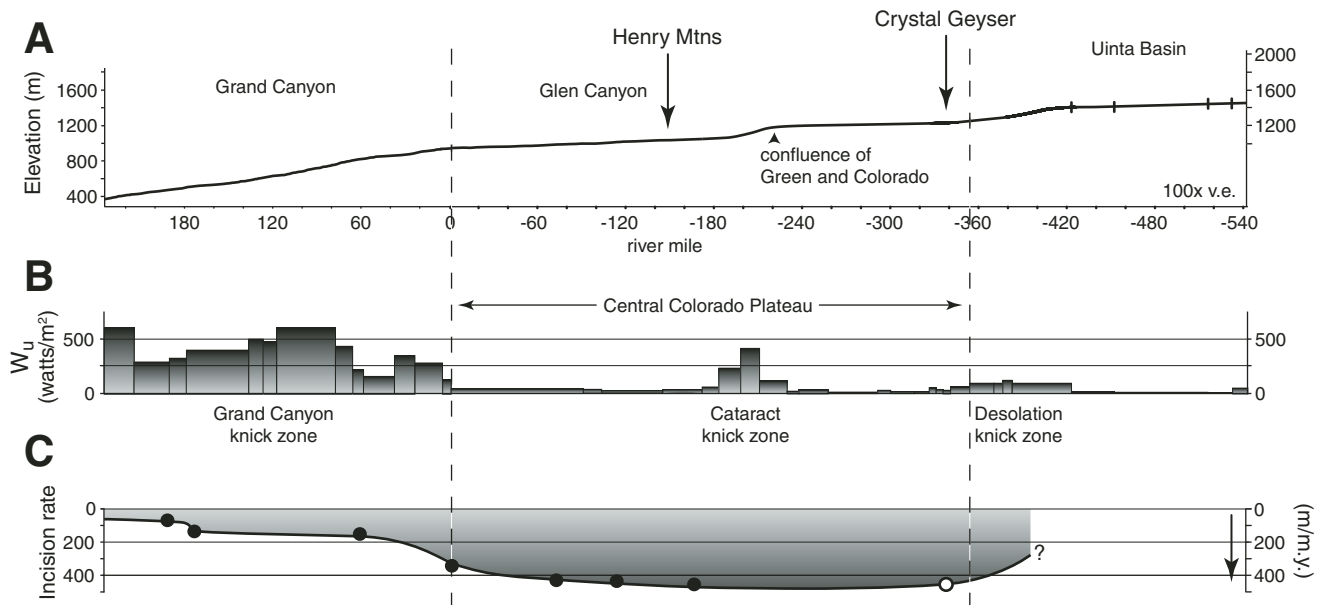


Figure 10. (A) the longitudinal profile of the Green-Colorado river system starting where the Green River crosses the Uinta Basin, through the Desolation knickzone, past Crystal Geyser to the confluence of the Green and Colorado Rivers at the head of Cataract Canyon, and then past the Henry Mountains through Glen Canyon and finally to the Grand Canyon knickzone. (B) Reach-averaged unit stream power from Pederson and Tressler (2012). (C) Trend of comparably calculated late Quaternary river incision rates (larger black dots) from Pederson et al. (2013a, 2013b), with the white-centered data point being the result for Crystal Geyser. Note the lack of correspondence between the broad-wavelength pattern of incision rate and shorter variations in river steepness or energy, with the most rapid regional incision occurring in broad, low-energy reaches like Crystal Geyser. Modified from Pederson et al. (2013b).



Figure 11. Navajo Sandstone at North Wash (Stop 1-2), with Utah 95 in the middle distance. Rock in lower right foreground is a thin lens of micritic limestone that was deposited in an interdunal pond. Contorted strata (arrow) are visible among cross-bedded dune deposits. Carmel Formation (Jc) and Quaternary cobbles (Qc) cap the Navajo Sandstone (Jn).

accumulated in perennial, interdune lakes. Monsoonal rains sustained the high water tables for millennia (Loope and Rowe, 2003; Loope et al., 2004).

At this stop, burrows ranging in diameter from a few mm to ~15 cm are abundant in both the structureless and the cross-bedded sandstones that lie in close proximity to the carbonate lenses. The largest burrows were likely made by tritylodonts—a group of long-bodied, herbivorous, scratch-digging therapsids (Winkler et al., 1991). These animals may have also generated *Brasilichnium* trackways, which are also common in the Navajo Sandstone (Rowland and Mercadante, 2014). Calcareous rhizoliths (Loope, 1988) are also present here.

Directions to next stop. Drive back to Utah 276 and continue south toward Bullfrog. After ~17 mi, look for a right turn onto a wide gravel road that leads to the Star Springs Campground and the south side of Mt. Hillers. When the road forks just before the campground entrance, keep left to go west. Stay right at the next fork. In ~0.8 mi, look for tracks on the right that head toward the mountain front.

Stop 1-3: Mount Hillers (37° 51.192' N, 110° 41.622' W)

At this stop, we will park at the base of Mt. Hillers and walk north to the mouth of one of the drainages on the south side of the mountain. Here, the Permian–Cretaceous section is exposed, dipping steeply against the side of a large laccolith (Fig. 12). Layer-parallel slip facilitated the dramatic changes in dip across this ~2 km section (Johnson and Pollard, 1973; Pollard and Johnson, 1973; Jackson and Pollard, 1988). Walking up one of these drain-

ages (getting higher in elevation) means going down-section to older and more deeply exhumed units. The very steep, unstable talus slopes preclude walking through the entire section to the laccolith itself, though there are several porphyry sills and dikes at relatively low elevation that we can examine.

In the Henry Mountains, laccoliths intruded the Permian–Cretaceous strata of the central Colorado Plateau during the Oligocene (Nelson et al., 1992), dramatically deforming the country rocks and uplifting them 1–2 km above the surrounding canyon country (Gilbert, 1877; Johnson and Pollard, 1973; Pollard and Johnson, 1973; Jackson and Pollard, 1988). The five main peaks in the mountain range (Ellen, Pennell, Hillers, Holmes, and Ellsworth; Fig. 13) are each cored by a central ‘master’ laccolith and a variety of satellite laccoliths, sills, and dikes intruded at varying stratigraphic levels (Fig. 13; Gilbert, 1877; Hunt et al., 1953). As noted by Gilbert (1877), there is a geographic pattern in the intrusion depths and extent of unroofing from north (Mt. Ellen) to south (the Little Rockies, Mt. Holmes and Mt. Ellsworth). It is unclear whether this differential exhumation is the result of the relative proximity to the Colorado River, or a difference in the pattern of intrusion coupled with relative erodibility of the igneous and sedimentary rocks.

Taking a multi-chronometer approach, Murray et al. (2016) used zircon U–Pb geochronology to date the Mt. Hillers laccolith (26 Ma), apatite fission-track analysis to identify the extent of the thermal aureole where heating exceeded ~100 °C for sufficient time to partially or fully reset the detrital apatite crystals, and apatite He analysis in that reset region to constrain the post-magmatic landscape evolution history. Here, that reset region

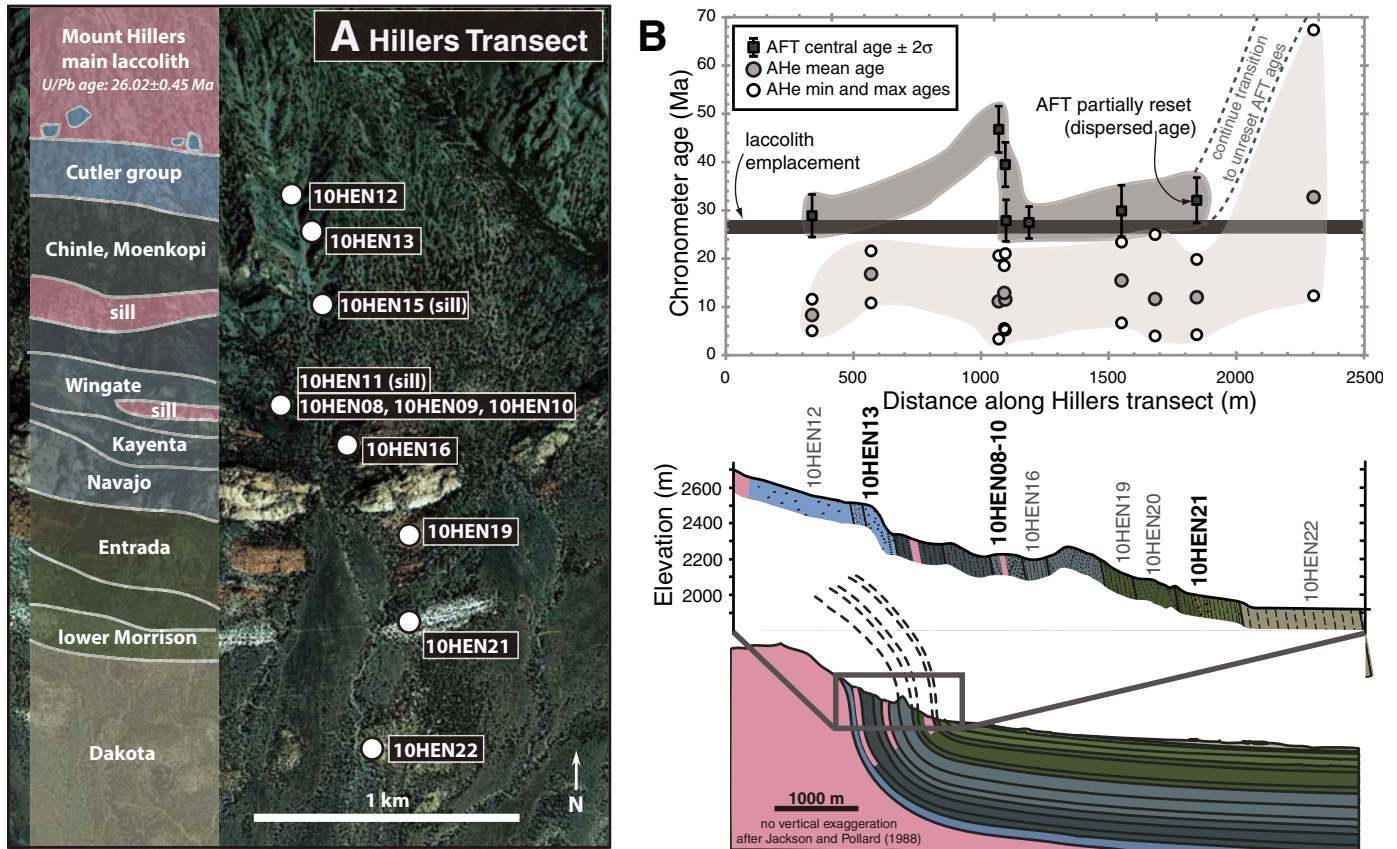


Figure 12. (A) Google Earth satellite image of the south side of Mt. Hillers overlaid with the sedimentary rocks exposed and dipping sub-vertically against the side of the laccolith. (B) Schematic cross section after Jackson and Pollard (1988) with locations of samples from Murray et al. (2016). Zircon U-Pb geochronology dates the Mt. Hillers laccoliths at 26 Ma. Apatite thermochronology results from the sandstones document the extent of resetting in the thermal aureole. Apatite fission-track (AFT) ages are within error of the intrusion age out to ~1.5 km, except for two samples in the Wingate Sandstone. Apatite He ages are younger than the magmatism up to ~2 km from the main laccolith and have significant inter- and intra-sample variability. Samples with ID labels have useful positive-slope He age-[eU] patterns that can be modeled for thermal history interpretations.

extends ~2 km from the main laccolith, through the tilted strata (Fig. 12).

The single-grain apatite He ages within the resetting zone on the south side of Mt. Hillers are variable, with ages as young as ca. 5 Ma and as old as 25 Ma (Murray et al., 2016; Fig. 12). In seven samples, five of which are from this transect, these form a distinctive positive-slope trend (Fig. 14A) when plotted against the apatite U-Th composition (combined into a single parameter, effective U, or $[eU] = [U] + 0.235[Th]$). This trend reflects the effects of the accumulation and annealing of radiation damage on the mobility of He in the apatite crystal lattice (Flowers et al., 2009; Gautheron et al., 2009), which is a useful source of apatite He age variability that we can model to retrieve tightly constrained thermal histories. Qualitatively, this trend suggests two periods of rock cooling, one in the late Oligocene, and the other since the latest Miocene. Quantitatively, the data require that after post-magmatic cooling, these rocks resided at temperatures no colder than 45 °C, in the apatite He partial retention zone, until at least 10 Ma; all the good-fit time-temperature paths require rock

cooling <5 Ma, most likely in the last 3–2 Ma (see Murray et al., 2016, for modeling details). The Oligocene cooling is clearly post-magmatic thermal relaxation; the Pliocene–Pleistocene cooling documents the erosion that cooled these rocks from ~45 °C to surface temperatures.

These results are best explained by erosion rates <30 m/m.y. prior to the late Pliocene and time-averaged rates of ~250–700 m/m.y. since then. It is clear that, like at Crystal Geyser, the 6–5 Ma integration of the Colorado River played a principal role in driving this erosional event by lowering the regional base level. There could be several additional factors driving recent rock cooling in the Henry Mountains. First, it is likely that the high-relief, high-elevation mountains experienced increased mountain snowpack (but not glaciation in the Henry Mountains, Hunt, 1956) and spring runoff during the wetter glacial periods of the Pleistocene. The steep, transport-limited bedrock channels that dominate the landscape are dominantly incised by seasonal snowmelt—and not summer monsoon runoff (Johnson et al., 2010)—which could explain the signal of

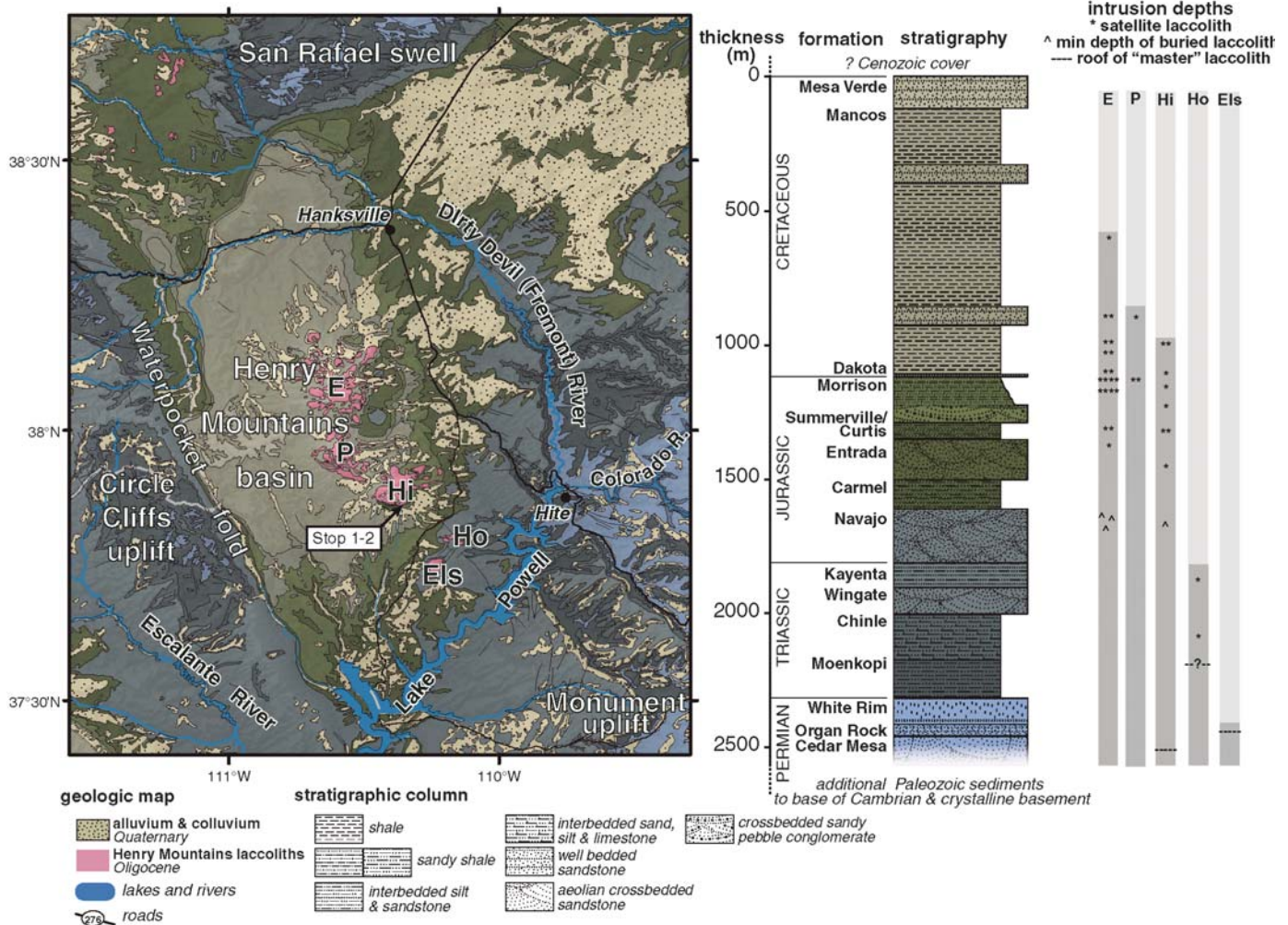


Figure 13. Geologic map of the Henry Mountains region with a stratigraphic column showing the average thickness and stratigraphy of the upper Paleozoic and Mesozoic strata (after Hunt et al., 1953; Jackson and Pollard, 1988; Hintze et al., 2000) into which the Henry Mountains laccoliths intruded. In the Henry Mountains basin, upper Cretaceous rocks are flat-lying and well preserved relative to the surrounding structural highs of the Waterpocket monocline and the San Rafael and Monument uplifts, where Triassic and Permian rocks dominate. The five main peaks of the Henry Mountains (E—Ellen, P—Pennell, Hi—Hillers, Ho—Holmes, Els—Ellsworth) are cored by clusters of Oligocene laccoliths that locally dome and deform the stratigraphy. The approximate intrusion depths of select laccoliths is shown to the right of the stratigraphic column for each of the five peaks (Gilbert, 1877; Hunt et al., 1953; Jackson and Pollard, 1988).

accelerated cooling in the Pleistocene. Additionally, cooler temperatures and snowmelt would have cooled and increased the groundwater fluxing downslope through these sandstones from the highest elevations (i.e., Whipp and Ehlers, 2007). This would have rapidly depressed bedrock temperatures, though erosion is still required to get these rocks to the surface. Finally, erosion rates could have accelerated as the laccoliths were unroofed and hard diorite clasts—the principal tools in the sandstone bedrock channels around the Henry Mountains today (Johnson et al., 2009; Cook et al., 2009)—became increasingly abundant.

Directions to next stop. We will now drive ~140 mi to Escalante for our overnight stay. We return to Utah 276 and drive south-

ward, past Tickaboo, and turn right (west) onto the Burr Trail; for full description, see Burr Trail. A 20 mi section of this route is unpaved; check road conditions before travel.

Overnight Stay 1 in Escalante

DAY 2

Directions to Stop 2-1. We will retrace 11 mi of the scenic route we took yesterday; turn right (southward) onto the Spencer Flat road (unpaved; with stop sign). The stop is ~7 mi from the turn-off. After ~4 mi, we will descend to Spencer Flat, proceed (on the main road), staying to the right at two splits in the road, and park

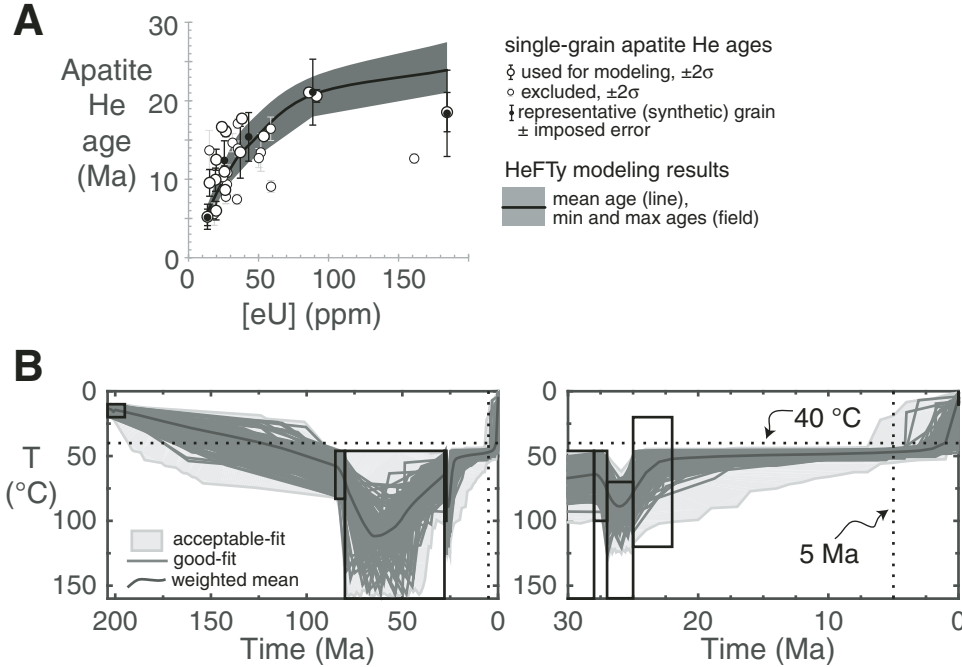


Figure 14. Thermal modeling results from the Wingate Sandstone on the south side of Mt. Hillers from Murray et al. (2016). (A) Single-grain apatite He results plotted against grain [eU] (symbols) and the good-fit thermal modeling results (gray field). This positive-slope trend is typical of the effects of radiation damage accumulation and annealing (RDAA, Flowers et al., 2009; Gautheron et al., 2009), which we model using the RDAA model in HeFTy (Ketcham, 2005; Flowers et al., 2009). (B) Time-temperature paths found to be acceptable (light-gray field) and good (dark-gray paths, $n = 100$) fits to the apatite He data. Model starts at depositional age. Right panel is zoomed into the last 30 m.y., the best constrained part of the sample thermal history. Black boxes—thermal history constraints from geology; dotted lines—reference lines for 40 °C and 5 Ma.

(on the right) at a small Navajo outcrop that is north of and within 0.25 mi of a high Navajo cliff (Fig. 15).

Stop 2-1: Spencer Flat (37° 42.046' N, 111° 22.216' W)

At this stop, we will walk westward along the Navajo outcrop ~0.5 mi, seeing abundant iron-oxide-cemented concretions with spheroidal and pipe-like shapes. The spheroids are the altered remains of dense siderite concretions. Alteration of the siderite was mediated by iron-oxidizing microbes (Weber et al., 2012; Figs. 16, 17).

Note that the oxide concretions in Figure 16 are the same size and shape as the precursor concretions. Later today we will see much larger concretions of diverse shapes that were altered in a very similar way. We call these types of structures *rimmed* concretions (Figs. 3A, 3B, 3C).

Iron-oxide, pipe-like structures at Spencer Flat project horizontally from vertical, NE-SW-oriented joints and are directed toward the southeast (Fig. 18). Prior to the oxidation that formed the pipe-like concretions, the precursor siderite was disseminated in the sandstone (Fig. 19). Because no aquifer is homogeneous, the first oxidizing water to reach the zone of disseminated siderite traveled as elongate fingers moving along paths with the highest permeability. Iron-oxidizing microbes established cylindrical biofilms around such conduits, forming “oxygen dams” along redox boundaries that were oriented parallel to flow direction in the aquifer, with oxygenated water inside and reducing water and siderite on the outside. As siderite was depleted near

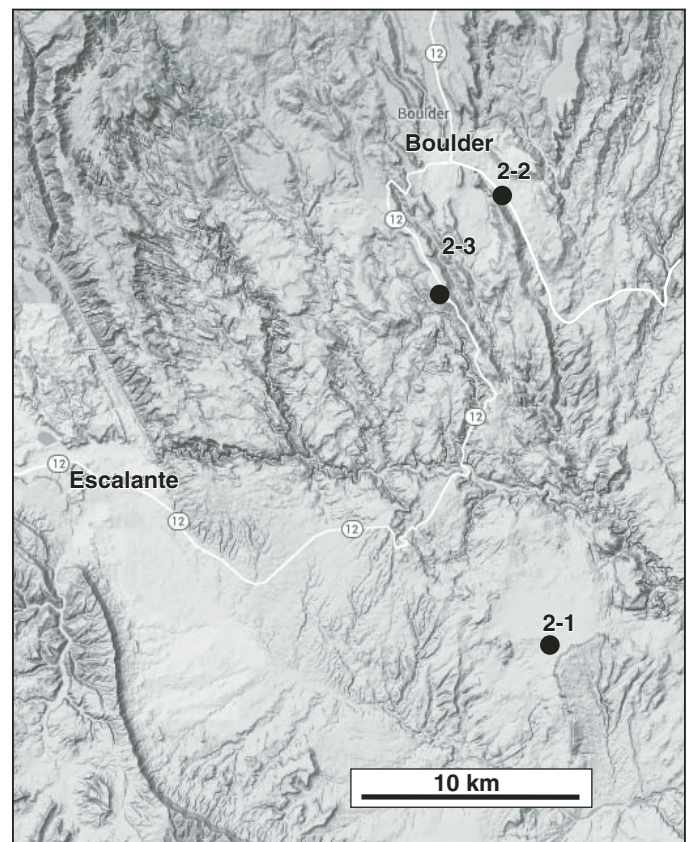


Figure 15. Locations of geologic stops, Day 2.

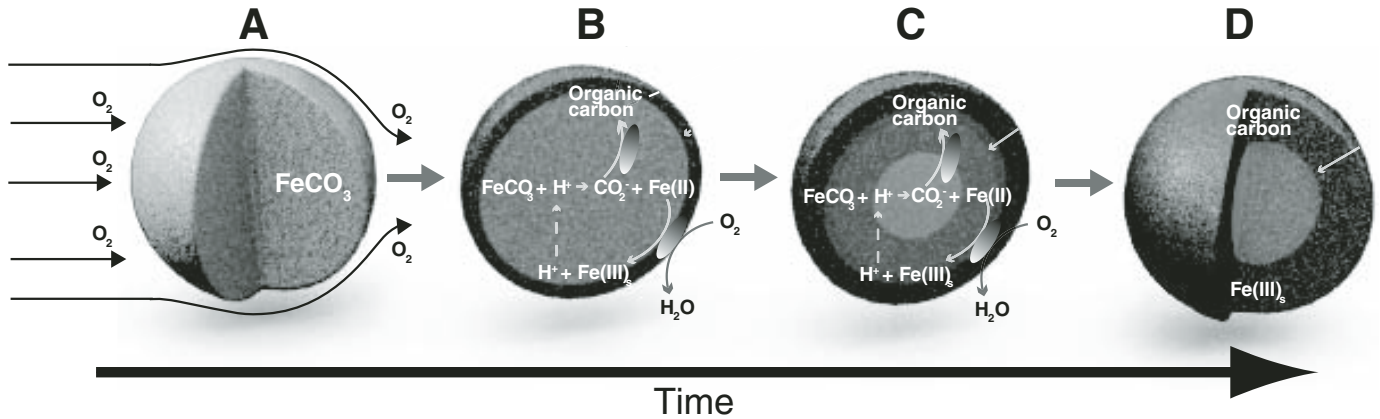


Figure 16. Conceptual model of oxidative iron biomineralization of Fe-rich concretions in an aquifer system. (A) Oxidizing fluids moving (gray arrows denote flow) through a sandstone matrix carrying O_2 expose siderite concretions to an oxidizing environment. (B) Microorganisms transform the Fe(II) carbonate concretions through the oxidation of Fe(II) coupled to the reduction of O_2 at the exterior of the Fe(III) oxide concretion. This produces protons (acidity) and precipitation of iron oxides: $4Fe(II) + O_2 + 10H_2O \rightarrow 4Fe(OH)_3 + 8H^+$. Acid promotes Fe(II) carbonate dissolution and release of aqueous Fe(II) and dissolved carbonate species: $H^+ + FeCO_3 \rightarrow Fe(II) + HCO_3^-$. Solid arrows denote reaction progress. Dissolved Fe(II) and carbonate/ CO_2 species freely diffuse toward the exterior of the concretion. Fe(II) is oxidized at the redox interface and carbonate/ CO_2 is autotrophically converted into organic carbon by iron-oxidizing microorganisms. (C) Continued microbial activity results in precipitation of Fe(III) oxides and inward growth of the outer rind. (D) The dissolved Fe(II) diffuses toward the exterior until Fe(II) carbonate is completely dissolved and oxidized, leaving an Fe(III) oxide rind and bleached sandstone interior. Gray denotes Fe(II) carbonate, and brownish-red denotes solid-phase Fe(III) oxides.

the biofilms and more oxidizing water arrived, they built a succession of dams (Fig. 19).

The iron-oxide pipes at Spencer Flat and the flow path of the modern Escalante River are oriented NW-SE (Figs. 18, 20). We do not think this is a coincidence. When iron- and CO_2 -bearing, reducing water flowed southeastward from the CO_2 -charged Escalante anticline (Loope et al., 2010), it crossed NE-SW-oriented joints and degassed, leading to siderite precipitation. At sites farther to the southeast, fer-

roan calcite precipitated (Figs. 20, 21). When the water later became oxygenated, the siderite was altered to iron oxide (Fig. 21), but the ferroan calcite remained unaltered because autotrophic, iron-oxidizing microbes cannot derive sufficient energy from its oxidation to sustain themselves (Loope et al., 2010). As Colorado Plateau uplift continued, the Escalante River dissected the Navajo Sandstone, and the iron-oxide- and ferroan-calcite-cemented concretions entered the vadose zone and became exposed on canyon walls.

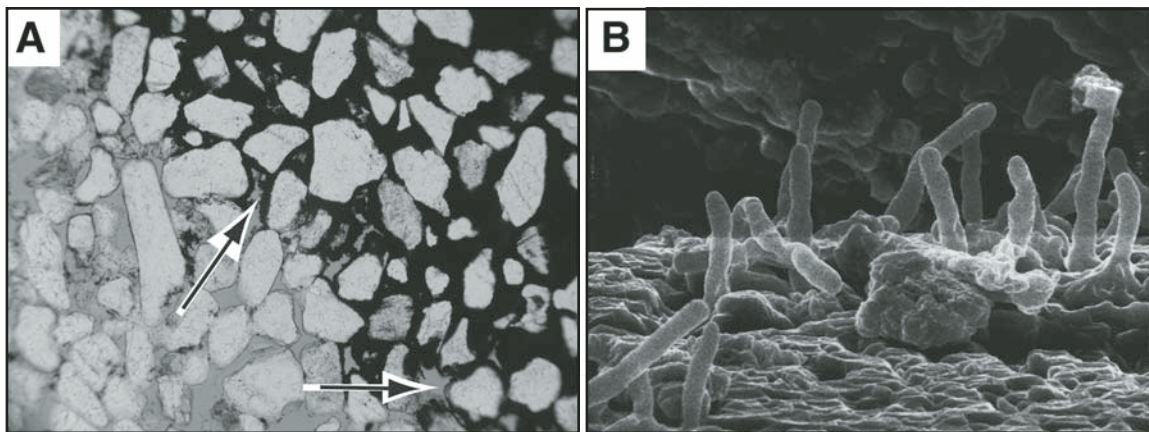


Figure 17. (A) Thin section from the Navajo Sandstone showing pore spaces at the inner edge of an iron-oxide-cemented rind on a spheroidal concretion. Field of view ~500 microns. (B) SEM image of microbes in the void space between two sand grains at the inner edge of the iron-oxide rind of a small, spheroidal concretion from the Navajo Sandstone. Tubules are 2 microns in diameter (Weber et al., 2012).

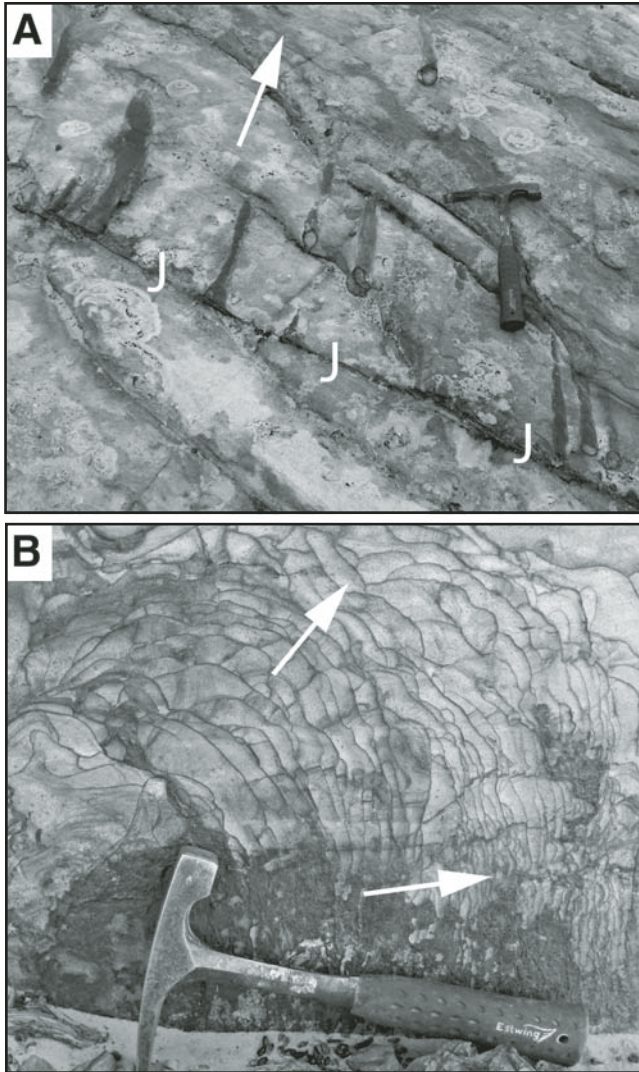


Figure 18. (A) Pipe-like concretions on a nearly horizontal outcrop. Pipes project southeastward (white arrow; see Fig. 20 for map showing paleoflow directions) from a joint (J) in the Navajo Sandstone at Spencer Flat. (B) Vertical outcrop exposing joint plane. Pipe-like concretions nucleated at this joint, elongated southeastward (into the photo), and accreted radially (white arrows) as concentric rings (compare Fig. 19H).

Directions to next stop. Return to Utah 12 and turn right (northeast) toward Boulder. We will likely take a lunch break at Calf Creek Recreation area (on left). In Boulder, turn right onto the Burr Trail and drive ~1.5 mi, and then park on right under large cottonwood tree.

Stop 2-2: Burr Trail, East of Boulder, Utah (37° 53.305' N, 111° 24.064' W)

Here we will see concretions much larger than the spheroids at our last stop, Spencer Flat. Like the spheroids, these are rinded concretions (Fig. 22B), but because of their larger size, joints

commonly cut these ovoid to tabular concretions. Many of the joints here are slope-parallel sheet fractures with origins similar to those in Yosemite National Park (Martel, 2011; Fig. 22A).

At this site and at Stop 2-3, the precursor (siderite) concretions pre-dated the joints, and nearly all joints pre-dated the oxidation of the siderite (Fig. 23). Joints controlled the flow of oxidizing waters, and, therefore, the positions of redox boundaries. Biofilms that occupied these boundaries produced thick bands of iron-oxide cement that parallel the joints. Two aims of future research are: (1) to use the youngest joints to better characterize microbial habitats; and (2) to better understand how slope-parallel joints influence landscape development.

Directions to next stop: Return to Boulder and turn left (toward Escalante) at the stop sign. Drive south ~5 mi; turnoff to parking area is to the west (right) about halfway between mileposts 81 and 82.

Stop 2-3: Upper Calf Creek (37° 51.559' N, 111° 26.264' W)

This stop entails a 3-mi (round-trip) hike to Upper Calf Creek Falls. At its start, the trail steeply descends ~500 ft. Sand and grit on the sandstone bedrock can produce a dangerous ball-bearing effect. *Step on clean bedrock to prevent slipping.*

We will see many large in situ boxwork concretions on our hike into this young canyon (Fig. 24). As at the last stop, many of these concretions are cut by joints. The andesitic boulders at the parking area are the remains of Pleistocene slurry flows and stream deposits that filled a paleovalley. Cosmogenic isotopes indicate an exposure age of ~670 ka (Marchetti et al., 2012). The topography is now inverted: the former valley floor now stands ~200 m above the canyons of Calf Creek and Dry Hollow (Fig. 25); Marchetti et al. (2012) calculated a maximum incision rate of 307 m/m.y. for this locality.

Overnight Stay 2 in Escalante

■ **DAY 3**

Directions to Stop 3-1: We will travel west out of Escalante on Utah Highway 12 and ascend through the Cretaceous section. The Upper Valley oilfield is located southwest of Escalante. This oilfield produces from the Permian Kaibab Limestone and is notable for having a strong water drive that displaces the oil column to the southwest of the crest of the Upper Valley anticline. As we drive through the Cretaceous section, a number of large carbonate concretions are visible on the righthand side of the road. Much of this section is the lower portion of the Kaiparowits Formation, which is thickest in the area of Canaan Peak (just to the south of the road) and thins northward. This area is referred to as “The Blues” because of the characteristic bluish-gray color of the Kaiparowits sandstones (Eaton, 1991). Upon reaching the summit, the country opens up with exposures of the Eocene Claron Formation visible along the northern horizon. Shortly after leaving Tropic, we will cross the Paunsaugunt fault and ascend the Paunsaugunt Plateau.

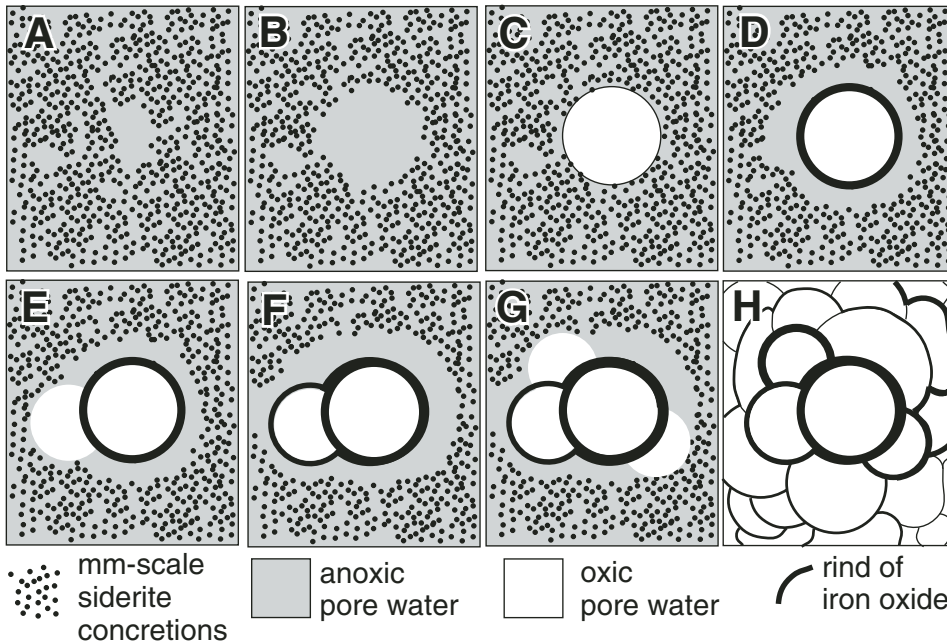


Figure 19. Formation of a coalesced mass of pipe-like concretions, viewed perpendicular to flow direction. (A) Degassing causes siderite cement to precipitate, forming thousands of small, disseminated spheroids just down flow of northeast-southwest-oriented joints. Aquifer is heterogeneous due to uneven distribution of small siderite spheroids. (B) Acidic, anoxic water enters a sparsely cemented zone and starts to dissolve spheroids, generating a positive feedback that leads to elongation and radial expansion of a conduit. (C) Oxygenated water reaches the conduit. Iron-oxidizing microbes colonize the perimeter of the conduit and start metabolizing Fe(II) to Fe(III), thereby initiating an iron-oxide-cemented “oxygen dam.” (D) Microbes thicken the dam and generate sufficient acid to dissolve the siderite concretions in the anoxic water just outside the rind. (E) Oxygenated water enters zone where siderite concretions have been removed.

(F, G) The new conduit is colonized and a new dam forms and starts to thicken. (H) All siderite is dissolved, and all anoxic water has been flushed from rock. The cluster, which expanded radially with dams thickening outward, records a unique, but decipherable series of events (from Loope et al., 2011, fig. 8).

At the intersection of Utah Highway 12 with U.S. Highway 89, proceed south on U.S. Highway 89 and begin to descend through the section. We will finally re-enter the Mesozoic between Orderville and Mt. Carmel Junction.

The distinctive reddish cliffs north of Kanab are the Vermillion Cliffs and consist largely of the Triassic Moenave Formation. The Moenave is temporally equivalent (roughly) to the Wingate Sandstone, but comprises largely fluvial and lacustrine sedimentary rocks in addition to some eolian deposits.

Upon reaching Kanab, proceed east on U.S. Highway 89 to a sandstone quarry located along the Shinarump Cliffs (Fig. 26).

Stop 3-1: Shinarump Member, Chinle Formation: Two Varieties of Wonderstone along the Shinarump Cliffs, East of Kanab (Private Land)

This quarry is used as a staging area for processing blocks of Shinarump sandstone into decorative stone. The blocks stored in this quarry were obtained from quarries elsewhere in the Kanab area. The wonderstone pattern comprises thick bands of iron-oxide mineralization that occludes pore space (referred to as iron-oxide cement or IOC), and more delicate bands of iron-oxide mineralization that coats sand grains but does not occlude pore space (referred to as iron-oxide stain or IOS).

In these blocks, we will see four features characteristic of the wonderstone pattern.

1. Bands of iron-oxide cement exhibit systematic orientations within any single block. In some blocks, the iron-oxide bands will be convex toward the interior of a block,

whereas in other blocks the IOC bands will be convex outward (Fig. 27).

2. Bands of iron-oxide stain will typically appear to be truncated by the convex side of bands of IOC, and will typically become asymptotic with the concave side of the bands of IOC.
3. Bleaching is typically observed on the convex side of the IOC, whereas iron staining is more pervasive on the concave side of the IOC (Fig. 27).
4. It is typical to observe bleached cores in blocks where the IOC is convex inward (Fig. 27).

These assemblages of iron-oxide-cemented and -stained rocks are typically and incorrectly referred to as “Liesegang.” As we shall see, the Liesegang phenomenon produces part (but not all) of the iron-oxide mineralization visible in these blocks.

The Liesegang phenomenon is a form of chemical self-organization that produces bands of insoluble precipitate from the mixing of two solutes. Liesegang bands obey a number of laws with respect to the spacing between bands, band width, and the timing of band formation (Antal et al., 1998). One of these laws is the spacing law (or Jablczynski law) (Jablczynski, 1923). The spacing law states that the ratio of the distances of two consecutive bands from the solution interface is given by

$$X_n/(X_{n-1}) \rightarrow 1+p, \quad (1)$$

where X_n and X_{n-1} are the distance of the n and $n-1$ bands, respectively, from the interface between the two solutions and p is a

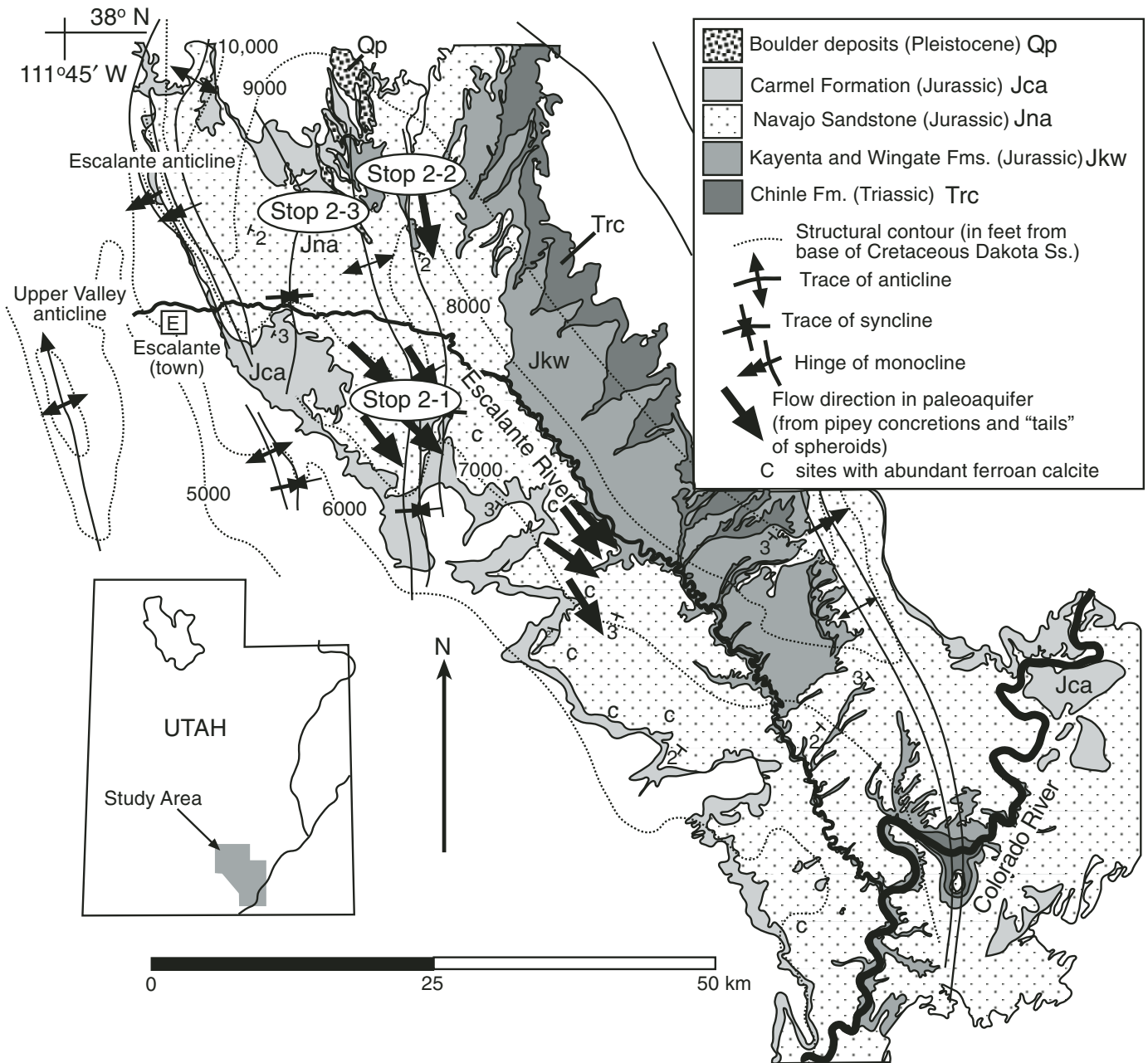


Figure 20. Geologic map of the area southeast of the Escalante anticline with locations of spheroids, boxworks, pipes, and paleoflow directions of oxidizing groundwater. From Loope et al. (2011, fig. 2).

constant between 0.05 and 0.4. Thus in Liesegang, the distance between bands must increase systematically as the distance from the solution interface increases.

We have applied this spacing test to IOC in blocks of Shinarump wonderstone. No single solution front can be assigned a priori to any series of IOC bands present within any block of Shinarump sandstone. On the other hand, if the bands are true Liesegang, the ratio defined in Equation 1 should still converge to $1+p$ if the distance is measured from any arbitrary point in

a direction approximately orthogonal to the IOC bands. If the bands are spaced randomly, then the value of p approaches zero and indicates that the Liesegang phenomenon is not a likely explanation for the band geometry and spacing. When we perform this analysis on bands of IOC, we find that the value of p approaches 0; in other words, the bands are spaced more or less evenly through the rock. Bands of IOS, on the other hand, do follow the Jablczynski spacing law and are likely Liesegang (Kettler et al., 2015).

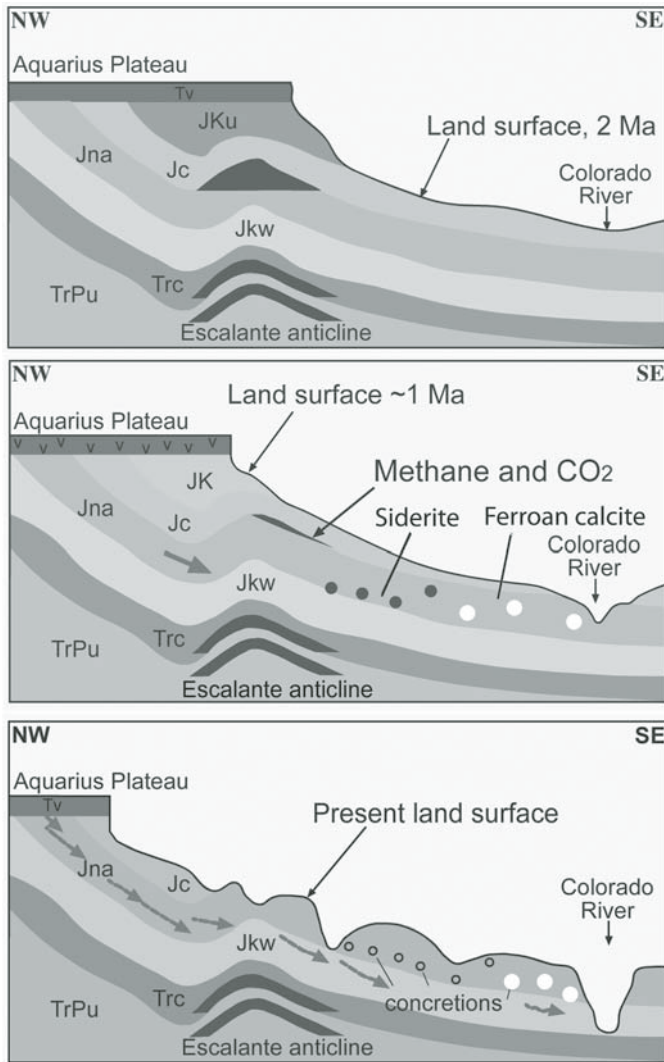


Figure 21. Evolution of concretions and landscape as hydrodynamic flow through the Escalante anticline sweeps trapped methane and CO_2 through down-dip sandstone. From Loope et al. (2010); available as Flash animation at ftp://rock.geosociety.org/pub/posit/2010/2010278_VideoDR1_final3-11.swf.

One feature of the bands of IOC that we will note in this quarry is that the distance between bands is greater if one of the bands is particularly thick. We tested this possibility (Kettler et al., 2015) and confirmed that if one is proceeding in the direction in which bands of IOC are convex, the distance from a thick band to the next band of IOC will be greater than it is from a thin band of IOC to the next succeeding band. We interpret this as evidence that the iron in these bands of IOC was derived from the space between the bands.

When we examine bands of IOC using scanning electron microscopy (SEM), we can find twisted strands of carbon and iron oxide similar to the iron-oxidizing microbe *Gallionella* (Kettler et al., 2015; Fig. 28). These twisted strands are consid-

ered to be support stalks for the iron-oxidizing microbes. Support stalks serve to keep the cell in an optimal position within the redox gradient, and prevent the cell from being covered in the iron-oxide minerals produced by its lithoautotrophic metabolism (C.S. Chan et al., 2011).

Our interpretation of the Shinarump wonderstone is that the sandstone was cemented locally with siderite during early methanogenic diagenesis beneath the river floodplain. The sandstone was fractured by joints during Basin and Range tectonism and infiltrated by oxygenated groundwaters during uplift of the Colorado Plateau. Iron-oxidizing bacteria colonized the redox interface between the oxidizing groundwaters and siderite cement. The microbes oxidized aqueous Fe^{2+} that diffused to the stabilized redox interface. The IOS marks reaction finger fronts (Ortoleva, 1994) produced as acid diffused away from newly precipitated ferric oxyhydroxide toward the reduced, siderite-cemented sandstone (Fig. 29). Each band of IOC represents a stabilized redox interface between the oxidizing portion of the aquifer and the more reduced, siderite-bearing portion of the system. Eventually, each stabilized interface in turn became unstable. It is possible that the microbial system lost the capacity to occlude oxidizing waters, or the iron-oxidation reactions might have become less exergonic with local depletion of Fe^{2+} as the siderite front became more distant, or the accumulation of acid may have driven local pH values below the range in which iron-oxidizing bacteria could thrive. In any event, a new interface was established and colonized by microbes. Finally, the geometry of the interface was such that microbes were able to completely isolate a volume of rock (Figs. 29M–29N) until all the reduced iron within it had been oxidized.

We interpret the IOS to have been produced during the breakthrough of oxygenated waters as the redox interface advanced within the rock. The interaction between residual Fe^{2+} absorbed on sand grains and invading oxygenated waters would mimic the geometry of the Liesegang phenomenon. In this interpretation (and in the absence of evidence for microbial activity in the precipitation of the IOS), the IOS is the product of apparently abiotic oxidation of Fe^{2+} that remains between a band of IOC and the siderite-cemented sandstone. Bleaching of IOS (Figs. 27, 29) must occur after the IOS is formed and may have been produced by iron-reducing bacteria that obtained electrons from the carbon that was fixed by the iron oxidizers.

Blocks in which the bands of IOC are convex toward the interior of the block are interpreted to be the products of oxidized groundwater infiltration along joints and the upper and lower contacts of Shinarump Member sandstones with confining mudstones. Those bands of IOC that are convex outward are actually pipe-like concretions produced as oxidizing groundwaters flowed through the Shinarump aquifer (cf. Fig. 19).

Directions to the next stop. We will drive ~55 mi south and west from Kanab. From the center of Kanab, take Highway 89A south to Fredonia. In Fredonia, we will take Highway 389 west, probably stopping at Pipe Spring National Monument (on the right)

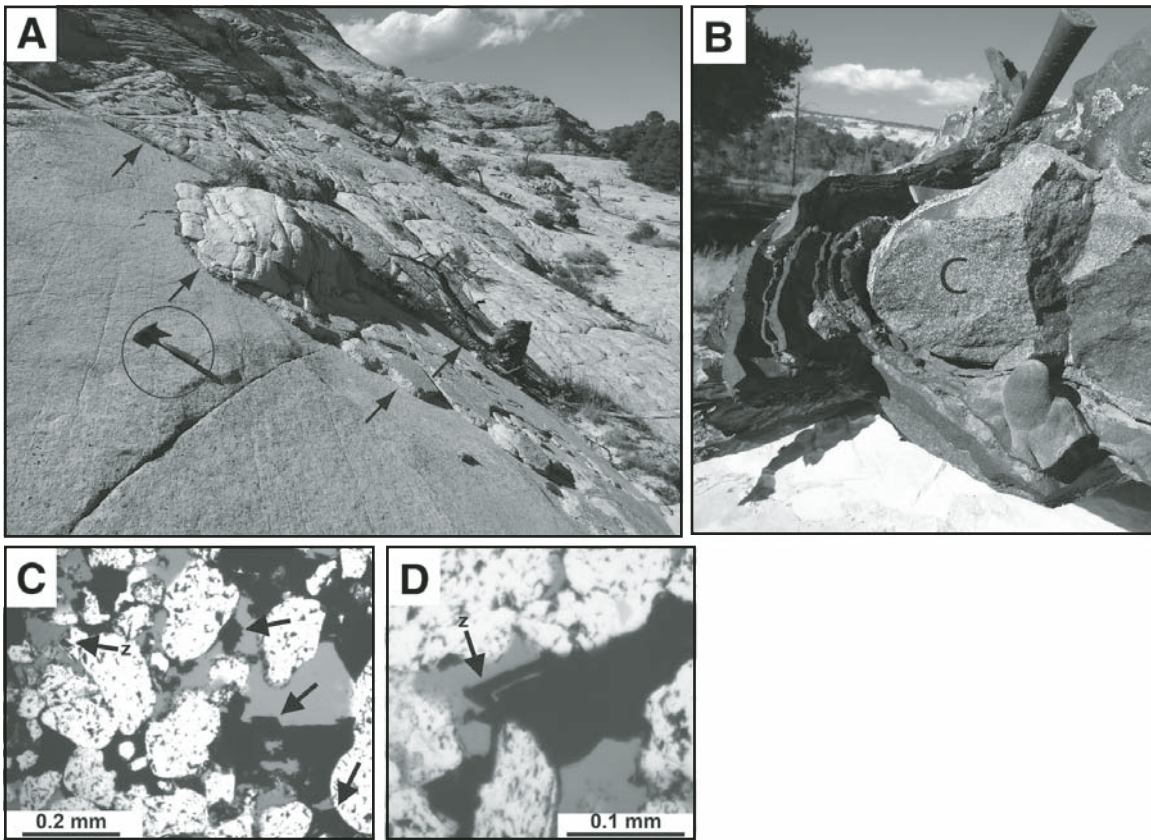


Figure 22. (A) Sheet fractures (arrows) in Navajo Sandstone that resemble those in granite at Yosemite National Park (cf. Martel, 2011). Rock hammer (circled) for scale. (B) Large iron-oxide concretion with abundant pseudomorphs in core (c) stone. (C, D) Photomicrographs of iron-oxide pseudomorphs after siderite.

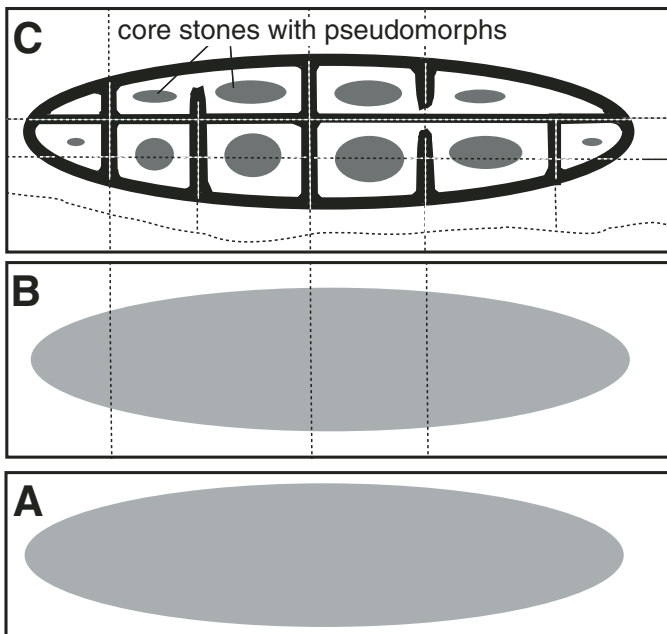


Figure 23. Evolution of large iron-oxide concretions. (A) Siderite concretion (gray) forms in reducing water at depth. (B) Joints (dashed lines) start to form as the rock cools (see Fossen, 2010, p. 87). (C) As the sandstone nears the surface, more fractures form, oxygenated water arrives, and all siderite is oxidized. As the siderite in the "moats" (white) around the cores dissolved, ferrous iron (Fe(II)) diffused to redox boundaries at the concretion perimeter and along both sides of joints where it was metabolized by microbes and precipitated as iron (Fe(III)) oxide (black). Nearly all joints pre-date siderite oxidation and control the position of iron-oxide accumulation, others cut (and therefore post-date) the iron oxide. Many of the largest concretions have "core stones" (dark gray) that contain abundant iron-oxide pseudomorphs after rhombic siderite crystals.

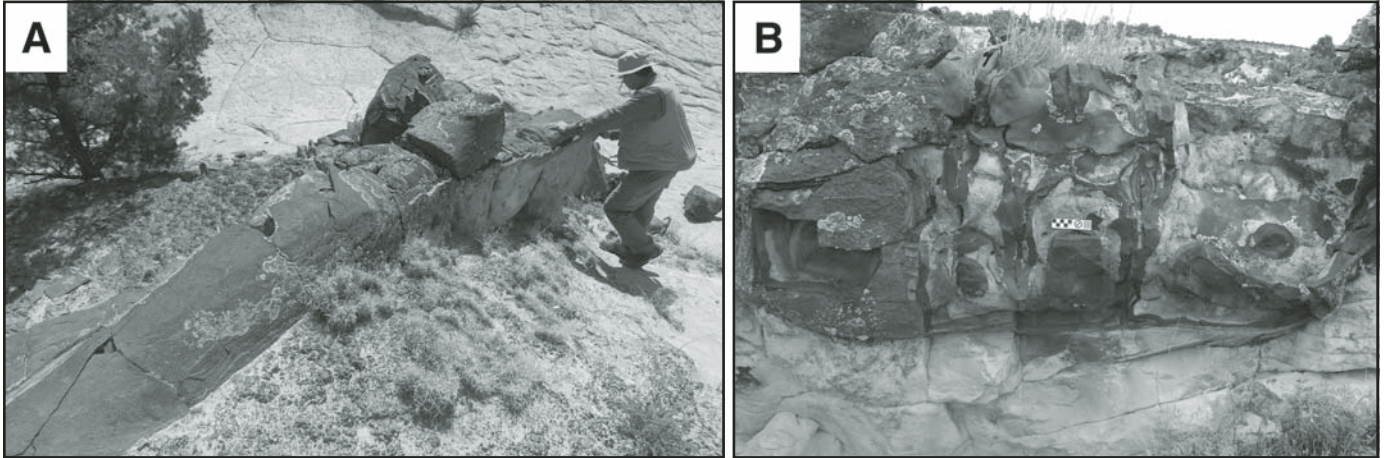


Figure 24. (A) Boxwork concretions with numerous joints and associated iron-oxide cements, Upper Calf Creek. (A) Large, elongated, rinded concretion enveloped in a thick (> 1 cm) sheath of iron-oxide-cemented sandstone. (B) Boxwork concretion with exterior sheath broken away, revealing internal compartments defined by cross-cutting joints each hosting a pair of partitions cemented by iron oxide (see Fig. 23). Ruler is 10 cm long.

for lunch. We will return to Highway 389 and travel west through Colorado City, Arizona, and Hildale, Utah. About 0.5 mi past the right turn marked “Scenic Byway,” we will turn left (west) beyond Colorado City, onto Little Creek Mesa Road (turn is at the end of the line of telephone poles on the left). After the road swings 90° to the left, start looking for a right turn marking Little Creek Mesa Road. Proceed along this gravel road to an abandoned quarry (Fig. 26).

Note: In late summer, southern Utah and the Arizona strip are affected by the North American monsoon (Adams and Comrie, 1997). The flash floods associated with these *heavy rains can be significant hazards*: one such flood occurred in September 2015 at the base of the Vermillion Cliffs, near Colorado City, and claimed 12 lives.

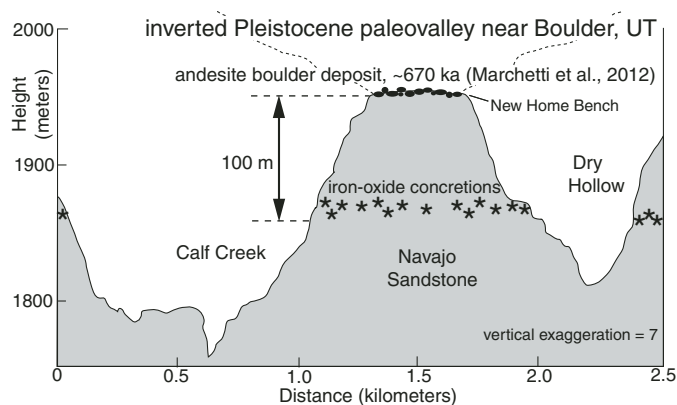


Figure 25. Inverted paleovalley near Boulder, Utah. Slurry-flow mass movements deposited boulders on what is now New Home Bench, armoring the floor of a Pleistocene valley. The canyons of Calf Creek and Dry Hollow were cut after the boulders were deposited (modified from Marchetti et al., 2012).

Stop 3-2: Shinarump Member: Wonderstone Quarry, Joints, and Rinded Mud Balls near Colorado City ($37^\circ 3.830' N, 113^\circ 7.852' W$)

This stop is located on private property with access (as of September 2016) administered by the Utah Department of Natural Resources under the Walk-in-Access program (<http://wildlife.utah.gov/walkinaccess/>). The property is designated as MidnightPropWashington2 in the Walk-in-Access Program database. Visitors should adhere to all regulations prescribed by the Utah Department of Natural Resources and check the status of the property before visiting the site.

This was a quarry where Shinarump sandstone was mined for use as a decorative stone and cored to produce coasters for drinks. In the quarry walls and in blocks of quarried sandstone, we will make six observations.

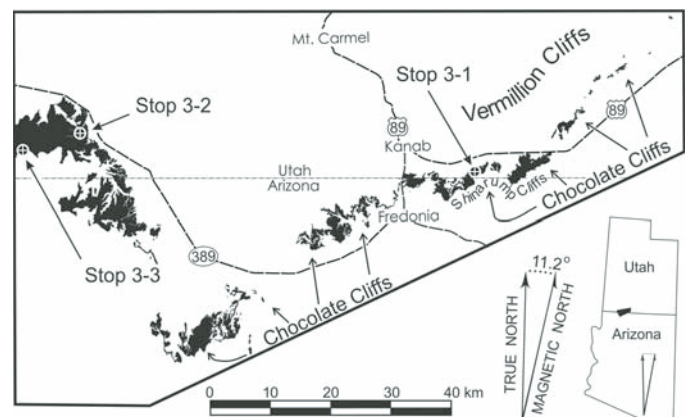


Figure 26. Location map of stops for Day 3 of field trip. Outcrop of Shinarump Member of Chinle Formation is shown in black.

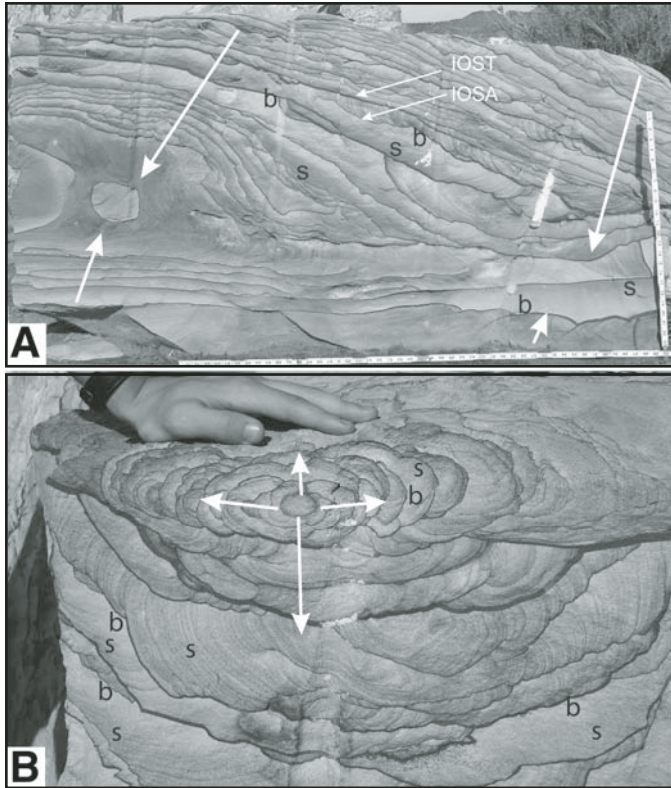


Figure 27. Image of two blocks of Shinarump Sandstone exhibiting “wonderstone” iron-oxide mineralization. A is an example of block in which the redox fronts advanced inward (as shown by the bold arrows), whereas B is an example of mineralization in which the redox fronts advance outward from the interior of the block (as shown by the white arrows). The lowercase b indicates rock that has been bleached, whereas the lower case s designates rock that has been stained with iron oxide. In A, the fine white arrow and letters IOST indicate an example of apparent truncation of iron-oxide stain (Liesegang) by the iron-oxide cement and the fine white arrow. The letters IOSTA indicate an example of iron-oxide stain that is apparently asymptotic to the concave side of a band of iron oxide cement.

1. The exposures in the quarry walls demonstrate that the Shinarump is a multistory sandstone. It was apparently deposited in a fluvial system with low accommodation as there is little preservation of the floodplain muds.
2. Rhombohedral patches of iron-oxide cementation that we interpret to be oxidized, poikilotopic siderite cements occur here; they are especially prominent in discarded drill core. These patches are evidence that the Shinarump was once cemented pervasively with siderite. This siderite was apparently the product of methanic diagenesis that occurred in a gaining stream (Burgess et al., 2016).
3. Rinded iron-oxide concretions are interpreted as transported clasts that were originally composed of sideritic mudstone (Loope et al., 2012; Burgess et al., 2016). These can be found in a number of quarried blocks and broken cores in this quarry. Although very little of the

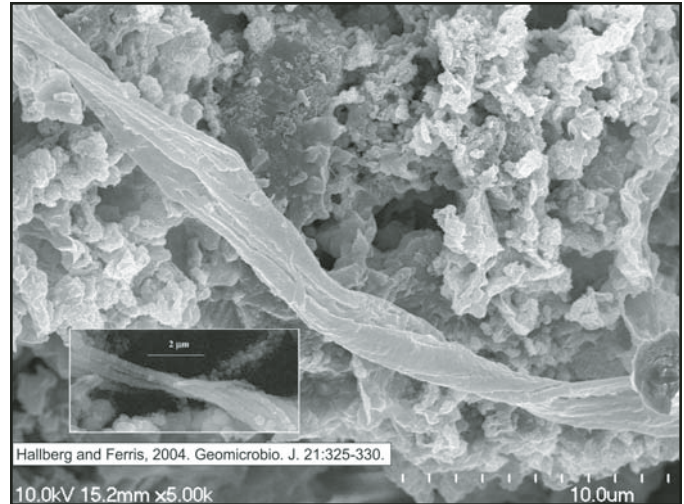


Figure 28. SEM image of Shinarump wonderstone showing a portion of a feature resembling modern *Gallionella*. Image illustrates the number of filaments in the stalk, the twisted nature of the stalk, and the relationship to iron-oxide cement. Inset shows published image of *Gallionella* (Hallberg and Ferris, 2004; Kettler et al., 2015).

floodplain mud is preserved, the presence of the rinded clasts is evidence that the early diagenetic environment in the floodplain muds was methanic. During later oxidation, the siderite concretion was converted to a porous interior and a dense iron-oxide rind.

4. Local small pyrite concretions can be observed in the quarry face and are evidence that trace amounts of sulfate were present during early diagenesis. It is important to note that the pyrite is preserved and exposed whereas the precursor to the rhombohedral pseudomorphs has been oxidized.
5. Joints control wonderstone mineralization in this quarry. At a number of points in the quarry walls, one can see oxidation fronts migrating inward from vertical fractures.
6. Steps in the development of wonderstone mineralization can be observed in the quarry face and in quarried blocks. One can observe where the oxidation front advanced from a fracture toward sandstone that now contains abundant rhombohedral accumulations of iron oxide (Fig. 30).

Directions to the next stop: Return to vehicle and drive westward toward the southwestern tip of Little Creek Mountain, following the main road and bearing left at Y-junctions. Turn left on small road at 37° 2.387' N, 113° 14.337' W and proceed to its end at the southern edge of Little Creek Mountain (Fig. 26). Stop 3-3 is located in the Little Creek Mountain Area of Critical Environmental Concern as designated by the Bureau of Land Management (see www.blm.gov/ut/st/en/fo/st_george/blm_special_areas/areas_of_critical/little_creek_mountain.html) for more information. Visitors should avoid vehicle travel off-road. Collection of anthropological artifacts is prohibited.

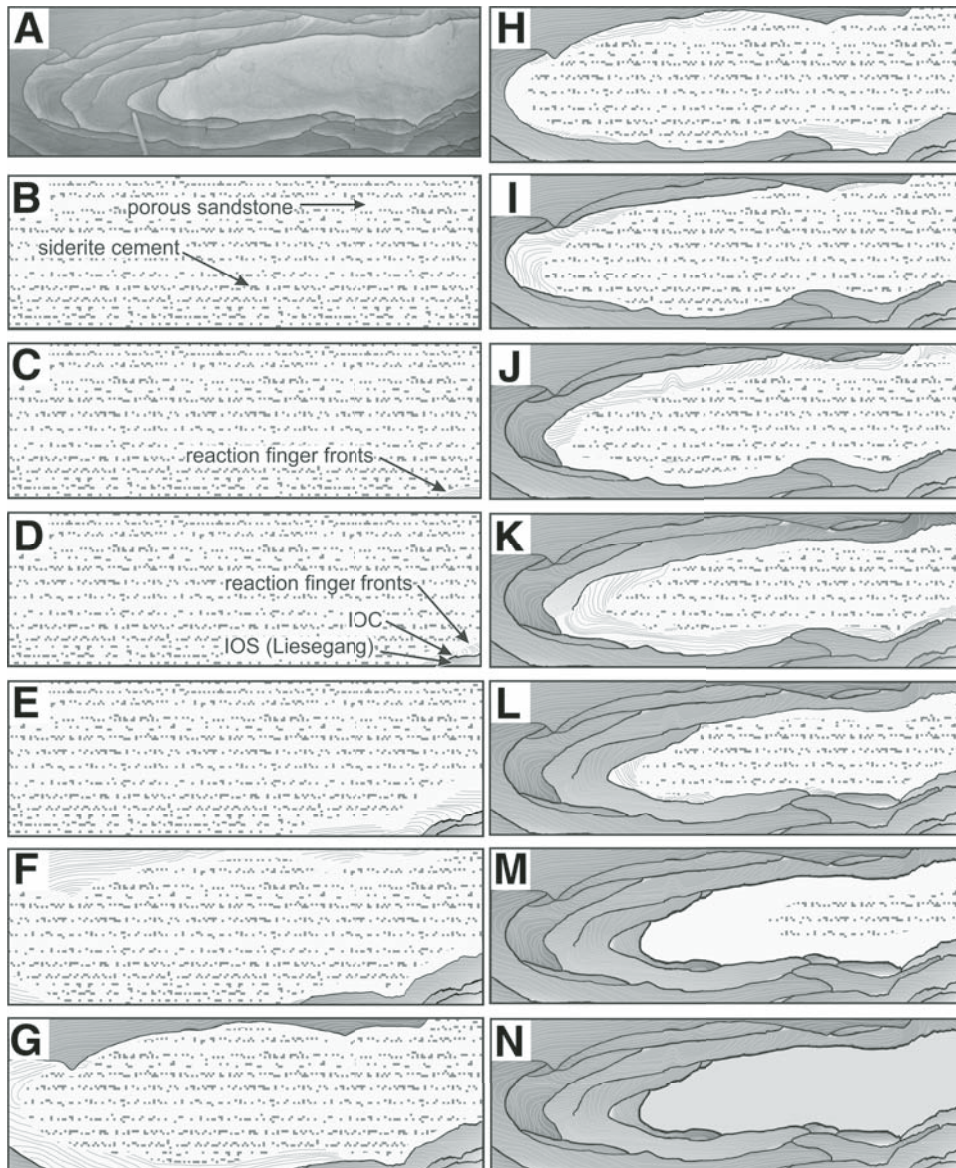


Figure 29. Image of wonderstone (A), followed by a sequence of diagrams that illustrate development of the wonderstone pattern (B–N). Initial porous sandstone is cemented locally by siderite. IOC (iron-oxide cement) initially forms out of field of view in C from iron derived from dissolution of siderite in lower right-hand corner. Arcuate lines in C represent reaction finger fronts (sensu Ortoleva, 1994). After abiotic oxidation of residual iron in lower right-hand corner to produce IOS (iron-oxide stain) (D), another redox interface is established and IOC begins to accumulate. The process repeats with the iron in each band of IOC being derived from the siderite in the sandstone on the convex side of each IOC band. Panels E–L illustrate the continuing development of the IOC and IOS whereas panels M and N illustrate the isolation and complete bleaching of the interior of the sandstone as the last band of IOC is formed.

Stop 3-3: Shinarump Member: Joint Control of Iron Oxides at Southern Edge of Little Creek Mesa (37° 2.328' N, 113° 14.215' W)

There are three significant observations that we want to make at this stop.

1) There is well-developed boxwork iron-oxide cementation in Shinarump sandstone (Fig. 31). The boxwork fractures have a consistent N- and NNW-dominated joint pattern similar to the pattern displayed on a much larger scale in the Navajo Sandstone of Zion National Park, 30 km to the northeast. In their analysis of the joints at Zion, Rogers et al. (2004) related the joints at Zion to the Miocene-to-Recent, counterclockwise rotation of regional extensional stresses in the eastern Basin and Range province. Iron-oxide accumulations along these relatively young joints

indicate that much (but not all) of the siderite that precipitated in the Triassic floodplain and channel sediments was preserved until the strata were lithified and exhumed. Studies of the Hurricane fault have shown that as the Basin and Range collapsed, the western Colorado Plateau (including the current study area) has been uplifted 1000–1500 m since the late Miocene (Anderson and Christianson, 1989; Biek et al., 2000). Oxidizing meteoric waters invaded the joints during Neogene exhumation and oxidized 200-m.y.-old siderite.

2) This site occurs at the contact between Shinarump sandstone and one of the most extensive mudstones preserved in the Shinarump. In the mudstone, we can find numerous iron-oxide concretions. Some of these concretions can weigh as much as 55 kg and are as large as 50 cm in diameter (Burgess et al., 2016). Where the original mineralogy is preserved, these concretions

are predominantly carbonate. Siderite, rhodochrosite, ankerite, and calcite comprise 56% of the concretion volume, whereas barite (20%), iron oxide (4%), and pyrite (3%) comprise much of the rest (Burgess et al., 2016). Many of these concretions are oxidized and fragment into characteristic dish-like chips. These iron-oxide-cemented chips occur as lag deposits in the Shinarump channels. We interpret the occurrence of the dish-like chips as evidence that much of the early diagenetic siderite was oxidized during the Triassic during arid periods. During these arid periods, the Shinarump fluvial system presumably comprised losing stream systems. As oxidizing waters infiltrated floodplain muds, any siderite concretions would have been oxidized. Subsequent erosion of these floodplain muds would have broken concretions and redeposited the fragments as channel lags.

The more abundant rinded and non-rinded iron-oxide concretions locally exhibit mineralization in the selvages of N- and NNW-trending fractures. The siderite in these concretions was preserved until Colorado Plateau exhumation allowed the invasion of oxidizing groundwater.

3) Pyrite concretions can be observed locally weathering out of the outcrop. The preservation of pyrite in a rock that is otherwise cemented with iron oxide is evidence that the rock must have been originally cemented with a reduced iron phase. That reduced iron phase must have had different oxidation kinetics than pyrite. We interpret this to be additional evidence that siderite was the precursor that reduced iron phase cementing the Shinarump. Siderite is oxidized by dissociation of the mineral into aqueous ferrous iron and bicarbonate. If the redox interface where ferrous iron will be oxidized is distant (mm to cm) from the mineral-water interface, then ferrous iron ions will diffuse to that interface, where they will be oxidized and trapped as ferric oxide. On the other hand, pyrite is typically dissolved and oxi-

dized upon attack by aqueous ferric iron. Pyrite oxidation cannot produce the wonderstone pattern or any similar patterns produced by cm-scale migration of iron. If the ferric iron is trapped as a solid phase, it is no longer available to oxidize pyrite. However, siderite dissolution is enhanced by the oxidation of ferrous iron at a redox boundary and entrapment as ferric oxide. Therefore, during pyrite oxidation, the redox boundary is positioned at the mineral-water interface, whereas siderite will dissolve readily when that boundary is several cm away.

Directions to the next stop: Return to the highway and turn left toward Hurricane, Utah. Descend the Hurricane fault, turn right at the first stop sign in town, then turn right onto Highway 9 at the first stoplight. Drive through La Verkin and then turn right (east) following Highway 9 toward Zion National Park and Springdale.

Overnight Stay 3 in Springdale

■ DAY 4

Directions to our next stop. We will drive 29 mi to Stop 4-1. From Springdale, we will go west on Highway 9, proceed through Rockville (see note below), and turn right on the Kolob Terrace Road just before reaching the town of Virgin, Utah. The prominent mesa on the right (north) is capped by basalt of the m.y.-old Lava Point flow and stands ~400 m above the Virgin River (immediately to the south). As we proceed, we will drive directly up the Grapevine basalt flows (0.2–0.3 Ma). Both the Lava Point and Grapevine flows moved down paleo-canyons. As we drive up the Grapevine flows, notice the deep canyons to our right and to our left—another great example of topographic inversion (Biek et al., 2000). We will drive up an

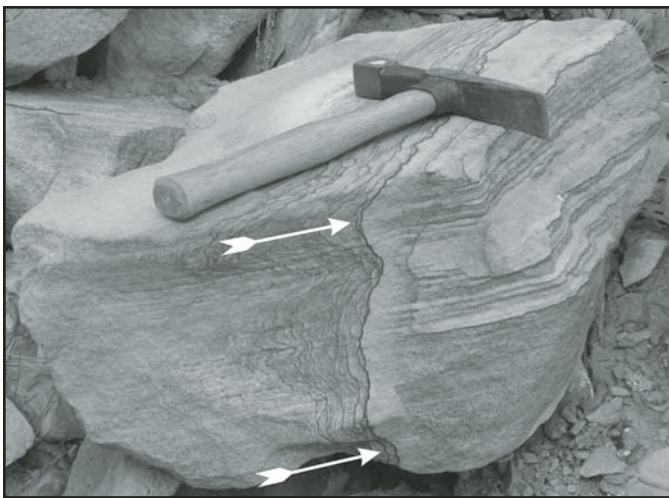


Figure 30. Image of wonderstone mineralization advancing on disseminated rhombohedral patches of iron-oxide cement that are interpreted to be oxidized pseudomorphs after siderite. Arrows show direction of oxygen advance.

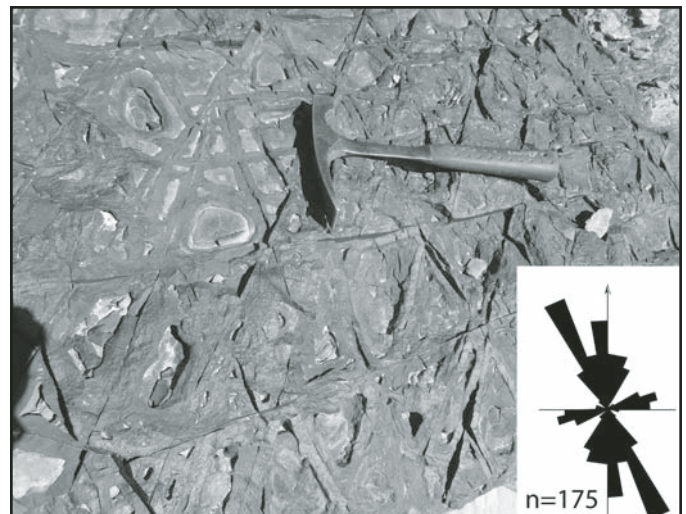


Figure 31. Boxwork formed via late diagenetic, iron-oxide mineralization along joints; top of fining-upward Shinarump sandstone, Little Creek Mesa.

impressive escarpment and park at the Wildcat Trailhead on the Lava Point flow, 16 mi from Virgin.

Note: At the west edge of Rockville on the north side of Highway 9, the Shinarump Member caps a near-vertical cliff, directly adjacent to residences. On 12 December 2013, a rock mass (estimated at 2700 tons, and positioned 375 ft (115 m) above road level) detached. One 500 ton boulder moved 750 ft (230 m) downslope and struck a home, causing two fatalities. *Rockfall hazard remains very high.*

Stop 4-1: Russell Gulch, North-Central Zion National Park (37° 20.394' N, 113° 4.547' W)

This stop entails a 2.5 mi walk over relatively even terrain. Initially, we will be walking on the flat upper surface of a valley-filling, Pleistocene lava flow—the Lava Point flow, dated at 1.02 ± 0.02 Ma (Fig. 32; Biek et al., 2000). Our destination is a

concretion-bearing outcrop of Navajo Sandstone that lies along the trail into Russell Gulch, toward The Subway, ~30 m below the basalt. The concretions are not the typical rinded concretions that we saw at Escalante. Instead, they are zoned and the iron did not move during their oxidation. We interpret the zones to reflect the changing iron content in reducing pore waters, while carbonate cement was being precipitated during growth of the precursor concretions. It is not clear to us why microbes did not mediate the oxidation and produce dense rinds. Across Russell Gulch to the east, at about this stratigraphic level in the Navajo Sandstone, there are similar zoned concretions that form hexagonal and rhombic crystal shapes (“sand crystals”) that are characteristic of carbonate euhedra (Fig. 33C).

Based on the topographic position of the toe of the Lava Point flow (400 m above the Virgin River), Biek et al. (2000) argued that, due to movements along the Hurricane fault, this part of Zion National Park has been uplifted 400 m in the last

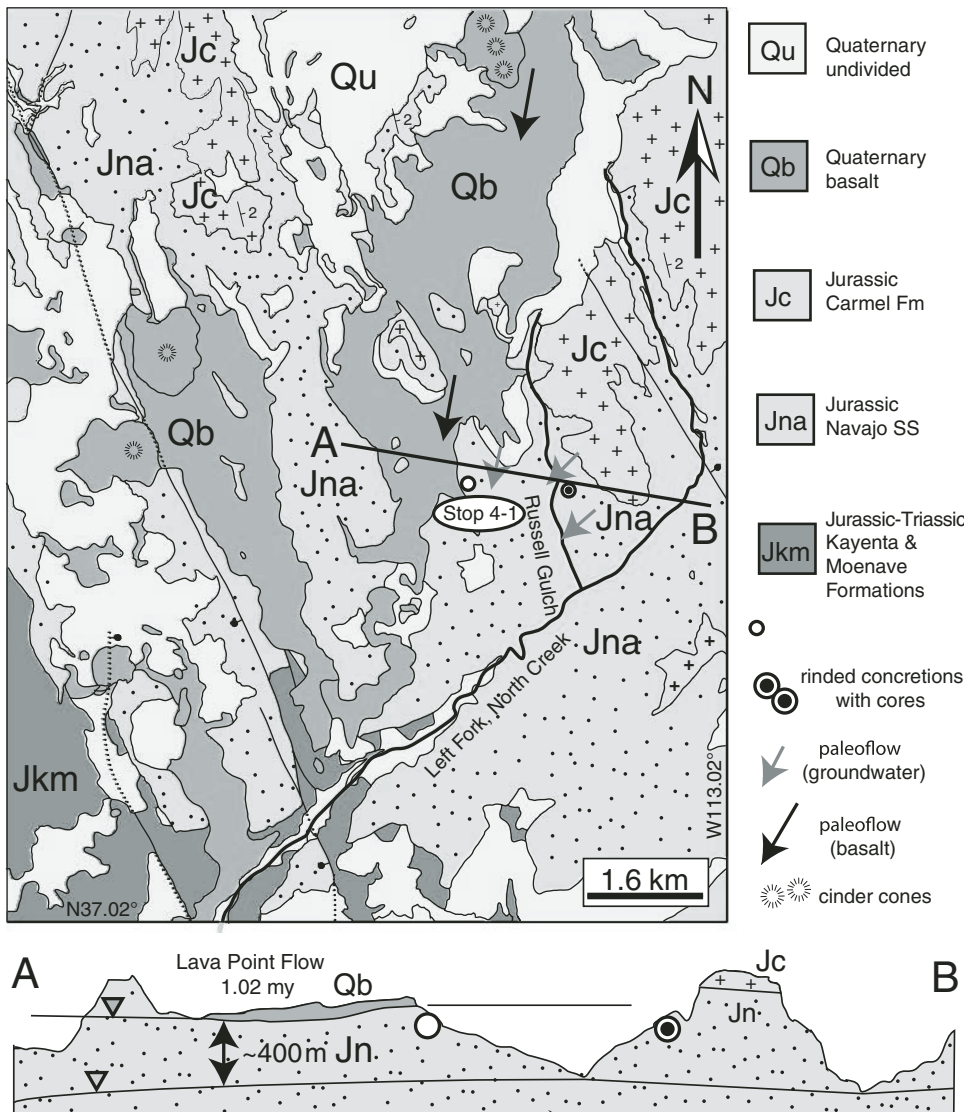


Figure 32. Geologic map and cross section show the distribution of Pleistocene basalt, Navajo Sandstone, capping strata of Carmel Formation, and concretion locations in west-central Zion National Park (Loope and Kettler, 2015, their fig. 12). One m.y. ago, basalt flowed southward down the paleovalley of North Creek. The modern canyons of North Creek and its tributaries (below Stop 4-1) were cut in the last 1 m.y., resulting in a topographic inversion. As a consequence of the post-basalt dissection, the groundwater table has dropped 400 m. Iron-oxide pipes and “tails” on concretions show that oxidizing groundwater in the Navajo aquifer flowed SSW, sub-parallel to both the lava flow and the modern drainage. Dates on iron oxide in concretions from Russell Gulch (see text) indicate oxidation took place less than 1 m.y. ago. These data are consistent with near-surface oxidation of siderite concretions. Modified from Interactive Geologic Map of Utah: <http://geology.utah.gov/apps/intgeomap/>.

1 m.y. The flow direction of paleo-groundwater, based on the orientation of nearby iron-oxide pipes and streaks (“comet-tails”) from spheroidal concretions, is parallel to the flow direction of Pleistocene lavas (Fig. 32; Loope and Kettler, 2015). U-Th/He dates on interior and exterior parts of iron-

oxide cements in the rinded Russell Gulch concretions are 0.53 ± 0.1 Ma (2 std err, $n = 11$) and 0.42 ± 0.1 Ma (2 std err, $n = 14$), respectively. All of this evidence is consistent with our hypothesis that rinded iron-oxide concretions in the Navajo Sandstone formed when oxidizing groundwater reached reduced-iron carbonate cements as these rocks were exhumed during uplift of the Colorado Plateau.

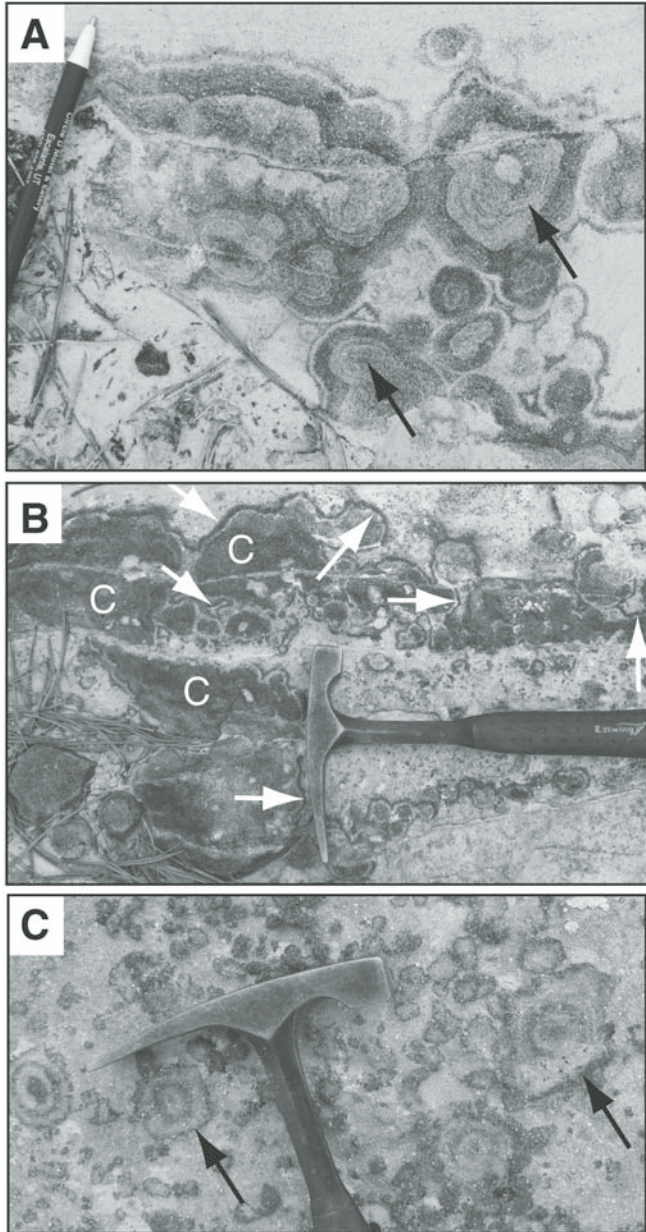


Figure 33. Concretions interpreted as the remains of iron-zoned, carbonate concretions after abiotic oxidation; Navajo Sandstone at Russell Gulch, Zion National Park. (A) Concretion with very thin zones (arrows; cf. Gautier, 1982, fig. 2). (B) Compound concretion that was (before oxidation) composed of iron-rich carbonate (siderite?) cores (c) that were followed by a thin, iron-poor (calcite?) zone, and, finally, by a thin, iron-rich zone (arrows). (C) Zoned (formerly carbonate) sand crystals with rhombic shapes (arrows; east side of Russell Gulch; see Loope and Kettler, 2015, fig. 9).

Directions to next stop: Return to Virgin and turn right on Utah 9. Descend the Hurricane fault just east of La Verkin, Utah, turn right on Utah 17, and proceed northward toward I-15 N. Stop 4-2 will be our lunch stop.

Stop 4-2: Kolob Section, Zion National Park (37° 26.115' N, 113° 12.080' W)

The impressive, red Navajo cliffs visible at this viewpoint notably lack evidence of bleaching by reducing fluids. Nielsen et al. (2009) showed that the transition from bleached to unbleached rock takes place in a very short distance (~2 km), but they could find no evidence for structural control. Iron-oxide concretions have not been reported from these outcrops. A possible explanation is that the buoyant, up-dip migrating fluids (see Fig. 5) never reached these rocks.

This is our last geologic stop. From here it is ~360 mi back to Grand Junction. We will follow I-15 northward along the eastern edge of the Basin and Range province, and then turn east on I-70, which will take us back across the High Plateau subprovince of the Colorado Plateau, along Sevier Valley (drains northward to Sevier Dry Lake, part of the Great Basin), through the San Rafael Swell (a large Laramide anticline), and back to Green River and Grand Junction.

ACKNOWLEDGMENTS

DBL and RMK thank Derek Burgess for his solid ideas and hard work on the Shinarump Member, and Ken Brown for his interest in wonderstone and his assistance with field access. Support for their research was provided by the National Aeronautics and Space Administration Nebraska Space Grant program, the University of Nebraska, Lincoln Vice Chancellor for Research, and the Committee for Research and Exploration (National Geographic Society). KEM acknowledges support from an NSF Graduate Research Fellowship, and awards from Achievement Rewards for College Scientists and the Philanthropic Education Organization. KEM and PWR acknowledge analytical support from Uttam Chowdhury and Erin Abel. Thorough reviews by Andrew Hutsky, Jesse Korus, and Steve Keller greatly improved the manuscript.

REFERENCES CITED

- Adams, D.K., and Comrie, A.C., 1997, The North American monsoon: Bulletin of the American Meteorological Society, v. 78, p. 2197–2213, doi:10.1175/1520-0477(1997)078<2197:TNAM>2.0.CO;2.

- Allin, D.L., 1993, Upper Valley, *in* Hill, B.G., and Bereskin, S.R., eds., Oil and Gas Fields of Utah: Utah Geological Association Publication 22, 192 p.
- Allis, R.G., Chidsey, T., Gwynn, W., Morgan, C., White, C., Adams, M., and Moore, J., 2001, Natural CO₂ reservoirs on the Colorado Plateau and Southern Rocky Mountains: Candidates for CO₂ sequestration, *in* Proceedings of 1st National Conference on CO₂ Sequestration: Washington, D.C., Department of Energy, National Energy Technology Laboratory.
- Anderson, R.E., and Christianson, G.E., 1989, Quaternary Faults, Folds, and Selected Volcanic Features in the Cedar City 1° × 2° Quadrangle, Utah: Utah Geological and Mineralogical Survey Miscellaneous Publication 89-6, scale 1:250,000, 29 p.
- Antal, T., Droz, M., Mangin, J., Rácz, Z., and Zrinyi, M., 1998, Derivation of the Matalon-Packter law for Liesegang patterns: The Journal of Chemical Physics, v. 109, p. 9479–9486, doi:10.1063/1.477609.
- Beitler, B., Chan, M.A., and Parry, W.T., 2003, Bleaching of Jurassic Navajo Sandstone on Colorado Plateau Laramide highs: Evidence of exhumed hydrocarbon supergiants?: Geology, v. 31, p. 1041–1044, doi:10.1130/G19794.1.
- Beitler, B., Parry, W.T., and Chan, M.A., 2005, Fingerprints of fluid flow: Chemical diagenetic history of the Jurassic Navajo Sandstone, southern Utah, U.S.A.: Journal of Sedimentary Research, v. 75, p. 547–561, doi:10.2110/jsr.2005.045.
- Bickle, M.J., 2009, Geological carbon storage: Nature Geoscience, v. 2, p. 815–818, doi:10.1038/ngeo687.
- Biek, R.F., Willis, G.C., Hylland, M.D., and Doelling, H.H., 2000, Geology of Zion National Park, Utah, *in* Sprinkel, D.A., Chidsey, T.C., and Anderson, P.B., eds., Geology of Utah's Parks and Monuments: Utah Geological Association Publication 28, p. 107–135.
- Black, B.D., and Hecker, S., compilers, 1999, Fault number 2473, Ten Mile graben faults, *in* Quaternary Fault and Fold Database of the United States: U.S. Geological Survey, <http://earthquakes.usgs.gov/hazards/qfaults>.
- Bryant, G., and Miall, A., 2010, Diverse products of near-surface sediment mobilization in an ancient aeolianite: Outcrop features of the early Jurassic Navajo Sandstone: Basin Research, v. 22, p. 578–590, doi:10.1111/j.1365-2117.2010.00483.x.
- Burgess, D.T., Kettler, R.M., and Loope, D.B., 2016, The geologic context of wonderstone—A complex, outcrop-scale pattern of iron-oxide cement: Journal of Sedimentary Research, v. 86, p. 498–511, doi:10.2110/jsr.2016.35.
- Burnside, N.M., Shipton, Z.K., Dockrill, B., and Ellam, R.M., 2013, Man-made versus natural CO₂ leakage: A 400 k.y. history of an analogue for engineered geological storage of CO₂: Geology, v. 41, p. 471–474, doi:10.1130/G33738.1.
- Bursztyn, N., Pederson, J.L., Tressler, C., Mackley, R.D., and Mitchell, K.J., 2015, Rock strength along a fluvial transect of the Colorado Plateau—Quantifying a fundamental control on geomorphology: Earth and Planetary Science Letters, v. 429, p. 90–100, doi:10.1016/j.epsl.2015.07.042.
- Carter, A., and Gallagher, K., 2004, Characterizing the significance of provenance on the inference of thermal history models from apatite fission-track data—A synthetic data study; *in* Bernet, M., and Spiegel, C., eds., Detrital Thermochronology: Geological Society of America. Special Paper, 378, p. 7–23, doi:10.1130/0-8137-2378-7.7.
- Chan, C.S., Fakra, S.C., Emerson, D., Fleming, E.G., and Edwards, K., 2011, Lithotrophic iron-oxidizing bacteria produce organic stalks to control mineral growth: Implications for biosignature formation: The ISME Journal, v. 5, p. 717–727, doi:10.1038/ismej.2010.173.
- Chan, M.A., and Bruhn, R., 2014, Dynamic liquefaction of Jurassic sand dunes: Processes, origins, and implications: Earth Surface Landforms and Processes, v. 39, p. 1478–1491, doi:10.1002/esp.3539.
- Chan, M.A., Parry, W.T., and Bowman, J.R., 2000, Diagenetic hematite and manganese oxides and fault-related fluid flow in Jurassic sandstones of southeastern Utah: The American Association of Petroleum Geologists Bulletin, v. 84, p. 1281–1310.
- Chan, M.A., Parry, W.T., Bowen, B.B., and Potter, S.L., 2011, Follow the water: Connecting a CO₂ reservoir and bleached sandstone to iron-rich concentrations in the Navajo Sandstone of south-central Utah, USA [Comment]: Geology, v. 39, no. 11, p. e250, doi:10.1130/G31983C.1.
- Colman, S.M., 1983, Influence of the Onion Creek salt diapir on the late Cenozoic history of Fisher Valley, southeastern Utah: Geology, v. 11, no. 4, p. 240–243, doi:10.1130/0091-7613(1983)11<240:IOTOC>2.0.CO;2.
- Cook, K.L., Whipple, K.X., Heimsath, A.M., and Hanks, T.C., 2009, Rapid incision of the Colorado River in Glen Canyon—Insights from channel profiles, local incision rates, and modeling of lithologic controls: Earth Surface Processes and Landforms, v. 34, p. 994–1010, doi:10.1002/esp.1790.
- Crossey, L.J., Fischer, T.P., Patchett, P.J., Karlstrom, K.E., Hilton, D.R., Newell, D.L., Huntoon, P., Reynolds, A.C., and de Leeuw, G.A.M., 2006, Dissected hydrologic system at the Grand Canyon: Interaction between deeply derived fluids and plateau aquifer waters in modern springs and travertine: Geology, v. 34, p. 25–28, doi:10.1130/G22057.1.
- Crossey, L.J., Karlstrom, K.E., Springer, A.E., Newell, D., Hilton, D.R., and Fisher, T., 2009, Degassing of mantle-derived CO and He from springs in the southern Colorado Plateau region—Neotectonic connections and implications for groundwater systems: Geological Society of America Bulletin, v. 121, p. 1034–1053, doi:10.1130/B26394.1.
- Davis, W.M., 1901, An excursion to the Grand Canyon of the Colorado: Bulletin of the Museum of Comparative Zoology, v. 38, p. 107–201.
- Delaney, P.T., and Gartner, A.E., 1997, Physical processes of shallow mafic dike emplacement near the San Rafael Swell, Utah: Geological Society of America Bulletin, v. 109, p. 1177–1192, doi:10.1130/0016-7606(1997)109<1177:PPOSMD>2.3.CO;2.
- Dickinson, W.R., and Gehrels, G.R., 2003, U-Pb ages of detrital zircons from Permian and Jurassic aeolian sandstones of the Colorado Plateau, USA: Paleogeographic implications: Sedimentary Geology, v. 163, p. 29–66, doi:10.1016/S0037-0738(03)00158-1.
- Dockrill, B., 2006, Understanding leakage from a fault-sealed CO₂ reservoir in east-central Utah: A natural analogue applicable to CO₂ storage [Ph.D. thesis]: Dublin, Ireland, Trinity College, 165 p.
- Dockrill, B., and Shipton, Z.S., 2010, Structural controls on leakage from a natural CO₂ geologic storage site: Central Utah, U.S.A: Journal of Structural Geology, v. 32, p. 1768–1782, doi:10.1016/j.jsg.2010.01.007.
- Doe, T.W., and Dott, R.H., Jr., 1980, Genetic significance of deformed cross-bedding—With examples from the Navajo and Weber Sandstones of Utah: Journal of Sedimentary Petrology, v. 50, p. 793–812.
- Eaton, J.G., 1991, Biostratigraphic framework for the Upper Cretaceous rocks of the Kaiparowits Plateau, southern Utah, *in* Nations, J.D., and Eaton, J.G., eds., Stratigraphy, Depositional Environments, and Sedimentary Tectonics of the Western Margin, Cretaceous Western Interior Seaway: Geological Society of America Special Paper 260, p. 47–64, doi:10.1130/SPE260-p47.
- Eichhubl, P., Davatzes, N.C., and Becker, S.P., 2009, Structural and diagenetic control of fluid migration and cementation along the Moab fault, Utah: The American Association of Petroleum Geologists Bulletin, v. 93, p. 653–681, doi:10.1306/02180908080.
- Eisenberg, L., 2003, Giant stromatolites and a supersurface in the Navajo Sandstone, Capitol Reef National Park, Utah: Geology, v. 31, p. 111–114, doi:10.1130/0091-7613(2003)031<0111:GSAASI>2.0.CO;2.
- Flowers, R.M., and Farley, K.A., 2012, Apatite ⁴He/³He and (U-Th)/He evidence for an ancient Grand Canyon: Science, v. 338, no. 6114, p. 1616–1619, doi:10.1126/science.1229390.
- Flowers, R.M., Ketcham, R.A., Shuster, D.L., and Farley, K.A., 2009, Apatite (U-Th)/He thermochronometry using a radiation damage accumulation and annealing model: Geochimica et Cosmochimica Acta, v. 73, p. 2347–2365, doi:10.1016/j.gca.2009.01.015.
- Fossen, H., 2010, Structural Geology: Cambridge, UK, Cambridge University Press, 463 p., doi:10.1017/CBO9780511777806.
- Fox, M., and Shuster, D.L., 2014, The influence of burial heating on the (U-Th)/He system in apatite: Grand Canyon case study: Earth and Planetary Science Letters, v. 397, p. 174–183, doi:10.1016/j.epsl.2014.04.041.
- Furuya, M., Mueller, K., and Wahr, J., 2007, Active salt tectonics in the Needles District, Canyonlands (Utah) as detected by interferometric synthetic aperture radar and point target analysis: 1992–2002: Journal of Geophysical Research, v. 112, B06418, doi:10.1029/2006JB004302.
- Garcia, V.H., and Reiners, P.W., 2015, Secondary Fe- and Mn-oxides associated with faults near Moab, Utah: Records of past fluid flow: Abstract V53E-3159 presented at 2015 Fall Meeting, AGU, 14–18 December 2015.
- Garden, I.R., Guscott, S.C., Burley, S.D., Foxford, K.A., Walsh, J.J., and Marshall, J., 2001, An exhumed palaeo-hydrocarbon migration fairway in a faulted carrier system, Entrada Sandstone of SE Utah, USA: Geofluids, v. 1, p. 195–213, doi:10.1046/j.1468-8123.2001.00018.x.
- Gautheron, C., Tassan-Got, L., Barbarand, J., and Pagel, M., 2009, Effect of alpha-damage annealing on apatite (U-Th)/He thermochronology: Chemical Geology, v. 266, p. 157–170, doi:10.1016/j.chemgeo.2009.06.001.
- Gautheron, C., Barbarand, J., Ketcham, R.A., Tassan-Got, L., van der Beek, P., Pagel, M., Pinna-Jamme, R., Couffignal, F., and Fialin, M., 2013, Chemical influence

- on α -recoil damage annealing in apatite: Implications for (U–Th)/He dating: *Chemical Geology*, v. 351, p. 257–267, doi:10.1016/j.chemgeo.2013.05.027.
- Gautier, D.L., 1982, Siderite concretions: Indicators of early diagenesis in the Gammon Shale (Cretaceous): *Journal of Sedimentary Petrology*, v. 52, p. 859–871.
- Gilbert, G.K., 1877, Report on the Geology of the Henry Mountains: Washington, D.C., Government Printing Office, 152 p. + plates, doi:10.5962/bhl.title.51652.
- Gilfillan, S.M.V., Ballentine, C.J., Holland, G., Blagburn, D., Lollar, B.S., Stevens, S., Schoell, M., and Cassidy, M., 2008, The noble gas geochemistry of natural CO₂ gas reservoirs from the Colorado Plateau and Rocky Mountain provinces, USA: *Geochimica et Cosmochimica Acta*, v. 72, p. 1174–1198, doi:10.1016/j.gca.2007.10.009.
- Gutiérrez, F., 2004, Origin of the salt valleys in the Canyonlands section of the Colorado Plateau: Evaporite-dissolution collapse versus tectonic subsidence: *Geomorphology*, v. 57, p. 423–435, doi:10.1016/S0169-555X(03)00186-7.
- Hallberg, R., and Ferris, F.G., 2004, Biomineralization by *Gallionella*: *Geomicrobiology Journal*, v. 21, p. 325–330, doi:10.1080/01490450490454001.
- Haszeldine, R.S., Quinn, O., England, G., Wilkinson, M., Shipton, Z.K., Evans, J.P., Heath, J., Crossey, L., Ballentine, C.J., and Graham, C.M., 2005, Natural geochemical analogues for carbon dioxide storage in deep geological porous reservoirs, a United Kingdom perspective: *Oil & Gas Science and Technology*, v. 60, p. 33–49, doi:10.2516/ogst:2005004.
- Heath, J.E., Lachmar, T.E., Evans, J.P., Kolesar, P.T., and Williams, A.P., 2009, Hydrogeochemical characterization of leaking carbon-dioxide-charged fault zones in east-central Utah, with implications for geologic carbon storage, in McPherson, B.J., and Sundquist, E.T., eds., *Carbon Sequestration and Its Role in the Global Carbon Cycle: American Geophysical Union Geophysical Monograph Series*, v. 183, p. 147–158, doi:10.1029/2006GM000407.
- Hintze, L.F., Willis, G.C., Laes, D.Y.M., Sprinkel, D.A., and Brown, K.D., 2000, Digital Geologic Map of Utah: Utah Geological Survey; <http://geology.utah.gov/apps/intgeomap/>.
- Hoffman, M.D., 2009, Mio-Pliocene erosional exhumation of the central Colorado Plateau, eastern Utah: New insights from apatite (U–Th)/He thermochronometry [M.S. thesis]: Lawrence, University of Kansas, 176 p.
- Horowitz, D., 1982, Geometry and origin of large-scale deformation structures in some ancient windblown sand deposits: *Sedimentology*, v. 29, p. 155–180, doi:10.1111/j.1365-3091.1982.tb01717.x.
- Humphreys, E., Hessler, E., Dueker, K., Farmer, G.L., Erslev, E., and Atwater, T., 2003, How Laramide-age hydration of North American lithosphere by the Farallon slab controlled subsequent activity in the western United States: *International Geology Review*, v. 45, p. 575–595, doi:10.2747/0020-6814.45.7.575.
- Hunt, C.B., 1956, Cenozoic Geology of the Colorado Plateau: U.S. Geological Survey Professional Paper, v. 279, 97 p.
- Hunt, C.B., Averitt, P., and Miller, R.L., 1953, Geology and Geography of the Henry Mountains Region, Utah: A Survey and Restudy of One of the Classic Areas in Geology: U.S. Geological Survey Professional Paper 228, 234 p.
- Hunter, R.E., 1977, Basic types of stratification in small eolian dunes: *Sedimentology*, v. 24, p. 361–387, doi:10.1111/j.1365-3091.1977.tb00128.x.
- Hunter, R.E., 1981, Stratification styles in aeolian sandstones: Some Pennsylvanian to Jurassic examples from the Western Interior U.S.A., in Ethridge, F.G., and Flores, R.M., eds., *Recent and Ancient Nonmarine Depositional Environments: Models for Exploration: SEPM (Society of Sedimentary Geology) Special Publication 31*, p. 315–329, doi:10.2110/pec.81.31.0315.
- Huntoon, P.W., 1988, Late Cenozoic gravity tectonic deformation related to the Paradox salts in the Canyonlands area of Utah, in *Salt Deformation in the Paradox Region: Utah Geological and Mineral Survey Bulletin*, v. 122, p. 80–93.
- Jablczynski, K., 1923, La formation rythmique des précipités: Les anneaux de Liesegang: *Bulletin de la Société Chimique de France*, v. 33, p. 1592–1597.
- Jackson, M., and Pollard, D., 1988, The laccolith-stock controversy: New results from the southern Henry Mountains, Utah: *Geological Society of America Bulletin*, v. 100, p. 117–139, doi:10.1130/0016-7606(1988)100<0117:TLSCNR>2.3.CO;2.
- Jochems, A.P., and Pederson, J.L., 2015, Active salt deformation and rapid, transient incision along the Colorado River near Moab, Utah: *Journal of Geophysical Research—Earth Surface*, v. 120, no. 4, p. 730–744, doi:10.1002/2014JF003169.
- Johnson, A., and Pollard, D.D., 1973, Mechanics of growth of some laccolithic intrusions in the Henry Mountains, Utah, I: Field observations, Gilbert's model, physical properties and flow of the magma: *Tectonophysics*, v. 18, p. 261–309, doi:10.1016/0040-1951(73)90050-4.
- Johnson, J.P.L., Whipple, K.X., Sklar, L.S., and Hanks, T.C., 2009, Transport slopes, sediment cover, and bedrock channel incision in the Henry Mountains, Utah: *Journal of Geophysical Research*, v. 114, F02014, doi:10.1029/2007JF000862.
- Johnson, J.P.L., Whipple, K.X., and Sklar, L.S., 2010, Contrasting bedrock incision rates from snowmelt and flash floods in the Henry Mountains, Utah: *Geological Society of America Bulletin*, v. 122, p. 1600–1615, doi:10.1130/B30126.1.
- Kampman, N., Burnside, N.M., Shipton, Z.K., Chapman, H.J., Nicholl, J.A., Ellam, R.M., and Bickle, M.J., 2012, Pulses of carbon dioxide emissions from intracrustal faults following climatic warming: *Nature Geoscience*, v. 5, p. 352–358, doi:10.1038/ngeo1451.
- Kampman, N., Bickle, M., Wigley, M., and Dubacq, B., 2014, Fluid flow and CO₂-fluid-mineral interactions during CO₂-storage in sedimentary basins: *Chemical Geology*, v. 369, p. 22–50, doi:10.1016/j.chemgeo.2013.11.012.
- Karlstrom, K.E., Crow, R., Crossey, L.J., Coblenz, D., and Van Wijk, J.W., 2008, Model for tectonically driven incision of the younger than 6 Ma Grand Canyon: *Geology*, v. 36, p. 835–838, doi:10.1130/G25032A.1.
- Karlstrom, K.E., Lee, J.P., Kelley, S.A., Crow, R.S., Crossey, L.J., Young, R.A., Lazear, G., Beard, L.S., Ricketts, J.W., Fox, M., and Shuster, D.L., 2014, Formation of the Grand Canyon 5 to 6 million years ago through integration of older palaeocanyons: *Nature Geoscience*, v. 7, p. 239–244, doi:10.1038/ngeo2065.
- Ketchum, R.A., 2005, Forward and inverse modeling of low-temperature thermochronometry data: *Reviews in Mineralogy and Geochemistry*, v. 58, p. 275–314, doi:10.2138/rmg.2005.58.11.
- Kettler, R.M., Loope, D.B., and Weber, K.A., 2011, Follow the water: Connecting a CO₂ reservoir and bleached sandstone to iron-rich concentrations in the Navajo Sandstone of south-central Utah, USA [Reply]: *Geology*, v. 39, no. 11, p. e251–e252, doi:10.1130/G32550Y.1.
- Kettler, R.M., Loope, D.B., Weber, K.A., and Niles, P.B., 2015, Life and Liesegang: Outcrop-scale microbially induced diagenetic structures and geochemical self-organization phenomena produced by oxidation of reduced iron: *Astrobiology*, v. 15, no. 8, p. 616–636, doi:10.1089/ast.2015.1305.
- Kocurek, G., and Dott, R.H., 1983, Jurassic paleogeography and paleoclimate of the central and southern Rocky Mountain region, in Reynolds, M.W., and Dolly, E.D., eds., *Mesozoic Paleogeography of West-Central United States: Denver, SEPM Rocky Mountain Section, Rocky Mountain Paleogeography Symposium 2*, p. 101–116.
- Konhäuser, K.O., Hamade, T., Raiswell, R., Morris, R.C., Ferris, F.G., Southam, G., and Canfield, D.E., 2002, Could bacteria have formed the Precambrian banded iron formations?: *Geology*, v. 30, p. 1079–1082, doi:10.1130/0091-7613(2002)030<1079:CBHFTP>2.0.CO;2.
- Lazear, G., Karlstrom, K.E., Aslan, A., and Kelly, S., 2013, Denudation and flexural isostatic response of the Colorado Plateau and southern Rocky Mountain region since 10 Ma: *Geosphere*, v. 9, p. 792–814, doi:10.1130/GES00836.1.
- Levander, A., Schmandt, B., Miller, M.S., Liu, K., Karlstrom, K.E., Crow, R.S., Lee, C.-T.A., and Humphreys, E.D., 2011, Continuing Colorado plateau uplift by delamination-style convective lithospheric downwelling: *Nature*, v. 472, p. 461–465, doi:10.1038/nature10001.
- Loope, D.B., 1988, Rhizoliths in ancient eolianites: *Sedimentary Geology*, v. 56, p. 301–314, doi:10.1016/0037-0738(88)90058-9.
- Loope, D.B., and Kettler, R.M., 2015, The footprints of ancient CO₂-driven flow systems: Ferrous carbonate concretions below bleached sandstone: *Geosphere*, v. 11, p. 943–957, doi:10.1130/GES01094.1.
- Loope, D.B., and Rowe, C.M., 2003, Long-lived pluvial episodes during deposition of the Navajo Sandstone: *The Journal of Geology*, v. 111, p. 223–232, doi:10.1086/345843.
- Loope, D.B., Steiner, M.B., Rowe, C.M., and Lancaster, N., 2004, Tropical westerlies over Pangean sand seas: *Sedimentology*, v. 51, p. 315–322, doi:10.1046/j.1365-3091.2003.00623.x.
- Loope, D.B., Kettler, R.M., and Weber, K.A., 2010, Follow the water: Connecting a CO₂ reservoir and bleached sandstone to iron-rich concretions in the Navajo Sandstone of south-central Utah, USA: *Geology*, v. 38, p. 999–1002, doi:10.1130/G31213.1.
- Loope, D.B., Kettler, R.M., and Weber, K.A., 2011, Morphologic clues to the origin of iron-oxide-cemented concretions in the Navajo Sandstone,

- south-central Utah: *The Journal of Geology*, v. 119, p. 505–520, doi:10.1086/661110.
- Loope, D.B., Kettler, R.M., Weber, K.A., Hinrichs, N.L., and Burgess, D.T., 2012, Rinded iron-oxide concretions: Hallmarks of altered siderite masses of both early and late diagenetic origin: *Sedimentology*, v. 59, p. 1769–1781, doi:10.1111/j.1365-3091.2012.01325.x.
- Loope, D.B., Elder, J.F., Zlotnik, V.A., Kettler, R.M., and Pederson, D.T., 2013, Jurassic earthquake sequence recorded by multiple generations of sand blows, Zion National Park, Utah: *Geology*, v. 41, p. 1131–1134, doi:10.1130/G34619.1.
- Loope, D.B., Kettler, R.M., Weber, K.A., and Al-Kuisi, M., 2016, Columnar macrofossils built in sandstone by iron-oxidizing microbes [abs.]: International Association of Sedimentologists Annual Meeting, Marrakech.
- Lucchitta, I., 1972, Early history of the Colorado River in the Basin and Range province: *Geological Society of America Bulletin*, v. 83, p. 1933–1948, doi:10.1130/0016-7606(1972)83[1933:EHOTCR]2.0.CO;2.
- MacMinn, C.W., and Juanes, R., 2013, Buoyant currents arrested by convective dissolution: *Geophysical Research Letters*, v. 40, p. 2017–2022, doi:10.1002/grl.50473.
- Marchetti, D.W., Hynek, S.A., and Cerling, T.E., 2012, Gravel-capped benches above northern tributaries of the Escalante River, south-central Utah: *Geosphere*, v. 8, p. 835–853, doi:10.1130/GES00772.1.
- Martel, S.J., 2011, Mechanics of curved surfaces, with application to surface-parallel cracks: *Geophysical Research Letters*, v. 38, L20303, doi:10.1029/2011GL049354.
- McKnight, E.T., 1940, *Geology of the Area between Green and Colorado Rivers, Grand and San Juan Counties, Utah*: U.S. Geological Survey Bulletin, v. 908, 147 p.
- Montgomery, D.R., 2004, Observations on the role of lithology in strath terrace formation and bedrock channel width: *American Journal of Science*, v. 304, p. 454–476, doi:10.2475/ajs.304.5.454.
- Moucha, R., Forte, A.M., Rowley, D.B., Mitrovica, J., Simmons, N.A., and Grand, S.P., 2009, Deep mantle forces and the uplift of the Colorado Plateau: *Geophysical Research Letters*, v. 36, L19310, doi:10.1029/2009GL039778.
- Murray, K.E., Reiners, P.W., and Thomson, S.N., 2016, Rapid Plio-Pleistocene erosion in the central Colorado Plateau documented by apatite thermochronology from the Henry Mountains: *Geology*, v. 44, p. 483–486, doi:10.1130/G37733.1.
- Nelson, S.T., Davidson, J.P., and Sullivan, K.R., 1992, New age determinations of central Colorado Plateau laccoliths, Utah: Recognizing disturbed K-Ar systematics and re-evaluating tectonomagmatic relationships: *Geological Society of America Bulletin*, v. 104, p. 1547–1560, doi:10.1130/0016-7606(1992)104<1547:NADOC>2.3.CO;2.
- Nielsen, G.B., Chan, M.A., and Petersen, E.U., 2009, Diagenetic coloration facies and alteration history of the Jurassic Navajo Sandstone, Zion National Park, southwestern Utah, in Tripp, B., Krahulec, K., and Jordan, L., eds., *Geology and Geologic Resources and Issues in Western Utah*: Utah Geological Association, v. 38, p. 67–96.
- Nuccio, V.F., and Condon, S.M., 1996, Burial and Thermal History of the Paradox Basin, Utah and Colorado, and the Petroleum Potential of the Middle Pennsylvanian Paradox Formation: U.S. Geological Survey Bulletin 2000-O, 41 p.
- Ortoleva, P., 1994, *Geochemical Self-Organization*: New York, Oxford University Press, 432 p.
- Owen, G., 1996, Experimental soft-sediment deformation: Structures formed by the liquefaction of unconsolidated sands and some ancient examples: *Sedimentology*, v. 43, p. 279–293, doi:10.1046/j.1365-3091.1996.d01-5.x.
- Parrish, J.T., and Falcon-Lang, H.J., 2007, Coniferous trees associated with interdune deposits in the Jurassic Navajo Sandstone formation, Utah, USA: *Palaeontology*, v. 50, p. 829–843, doi:10.1111/j.1475-4983.2007.00689.x.
- Pederson, J.L., and Tressler, C., 2012, Colorado River long-profile metrics: The hunt for knickzones and their meaning: *Earth and Planetary Science Letters*, v. 345–348, p. 171–179, doi:10.1016/j.epsl.2012.06.047.
- Pederson, J.L., Mackley, R.D., and Eddleman, J.L., 2002, Colorado Plateau uplift and erosion evaluated using GIS: *GSA Today*, v. 12, no. 8, p. 4–10, doi:10.1130/1052-5173(2002)012<0004:CPUAEE>2.0.CO;2.
- Pederson, J.L., Cragun, W.S., Hidy, A.J., Rittenour, T.M., and Gosse, J.C., 2013a, Colorado River chronostratigraphy at Lee's Ferry, Arizona, and the central Colorado Plateau bull's-eye of incision: *Geology*, v. 41, p. 427–430, doi:10.1130/G34051.1.
- Pederson, J.L., Burnside, N., Shipton, Z., and Rittenour, T.M., 2013b, Rapid river incision across an inactive fault—Implications for patterns of erosion and deformation in the central Colorado Plateau: *Lithosphere*, v. 5, p. 513–520, doi:10.1130/L282.1.
- Pevear, D.R., Vrolijk, P.J., and Longstaffe, F.J., 1997, Timing of Moab fault displacement and fluid movement integrated with burial history using radiogenic and stable isotopes, in Hendry, J., Carey, P., Parnell, J., Ruffell, A., and Worden, R., eds., *Geofluids II '97: Contributions to the Second International Conference on Fluid Evolution, Migration and Interaction in Sedimentary Basins and Orogenic Belts*: Belfast, The Queen's University of Belfast, p. 42–45.
- Pollard, D., and Johnson, A.M., 1973, Mechanics of growth of some laccolithic intrusions in the Henry mountains, Utah, II: Bending and failure of overburden layers and sill formation: *Tectonophysics*, v. 18, p. 311–354, doi:10.1016/0040-1951(73)90051-6.
- Polyak, V., Hill, C., and Asmerom, Y., 2008, Age and evolution of the Grand Canyon revealed by U-Pb dating of water table-type speleothems: *Science*, v. 319, p. 1377–1380, doi:10.1126/science.1151248.
- Powell, J.W., 1873, Some remarks on the geological structure of a district of country lying north of the Grand Canyon of the Colorado: *American Journal of Science Online*, series 3, v. 5, no. 30, p. 456–465, doi:10.2475/ajs.s3-5.30.456.
- Rahl, J.M., Reiners, P.W., Campbell, I.H., Nicolescu, S.A., and Charlotte, M., 2003, Combined single-grain (U-Th)/He and U/Pb dating of detrital zircons from the Navajo Sandstone, Utah: *Geology*, v. 31, p. 761–764, doi:10.1130/G19653.1.
- Reiners, P.W., Chan, M.A., and Evenson, N.S., 2014, (U-Th)/He geochronology and chemical compositions of diagenetic cement, concretions, and fracture-filling oxide minerals in Mesozoic sandstones of the Colorado Plateau: *Geological Society of America Bulletin*, v. 126, no. 9–10, p. 1363–1383, doi:10.1130/B30983.1.
- Riese, D.J., Hasiotis, S.T., and Odier, G.P., 2011, Synapsid burrows and associated trace fossils in the Lower Jurassic Navajo Sandstone, southeastern Utah, U.S.A., indicates a diverse community living in a wet desert ecosystem: *Journal of Sedimentary Research*, v. 81, p. 299–325, doi:10.2110/jsr.2011.25.
- Rogers, C.M., Douglas, A.M., and Engelder, T., 2004, Kinematic implications of joint zones and isolated joints in the Navajo Sandstone at Zion National Park, Utah: Evidence for Cordilleran relaxation: *Tectonics*, v. 23, TC1007, doi:10.1029/2001TC001329.
- Rowland, S.M., and Mercadante, J.M., 2014, Trackways of a gregarious, dunefield-dwelling Early Jurassic therapsid in the Aztec Sandstone of southern Nevada: *Palaios*, v. 29, p. 539–552, doi:10.2110/palo.2013.067.
- Rowley, P.D., Cunningham, C.G., Anderson, J.J., Steven, T.A., Workman, J.B., and Sneek, L.W., 2002, *Geology and mineral resources of the Marysvale volcanic field, southwestern Utah*: Cedar City, Utah, Geological Society of America Field Guide, Rocky Mountain Section Annual Meeting, in Lund, W.R., ed., *Field Guide to Geologic Excursions in Southwestern Utah and Adjacent Areas of Arizona and Nevada*: U.S. Geological Survey Open-File Report 02-172, p. 131–170.
- Schulze, D.J., Davis, D.W., Helmstaedt, H., and Joy, B., 2015, Timing of the Cenozoic “Great Hydration” event beneath the Colorado Plateau: Th-Pb dating of monazite in Navajo volcanic field metamorphic eclogite xenoliths: *Geology*, v. 43, no. 8, p. 727–730, doi:10.1130/G36932.1.
- Shipton, Z.K., Evans, J.P., Kirschner, D., Kolesar, P.T., Williams, A.P., and Heath, J., 2004, Analysis of CO₂ leakage through “low-permeability” faults from natural reservoirs in the Colorado Plateau, east-Central Utah, in Baines, S.J., and Worden, R.H., eds., *Geological Storage of Carbon Dioxide*: Geological Society, London, Special Publication 233, p. 3–59.
- Shipton, Z.K., Evans, J.P., Dockrill, B., Heath, J., Williams, A., Kirschner, D., and Kolesar, P.T., 2005, Natural leaking CO₂-charged systems as analogs for failed geologic storage reservoirs, in Thomas, D.C., and Benson, S.M., eds., *Carbon Dioxide Capture for Storage in Deep Geologic Formations, Volume 2*: Amsterdam, Elsevier, p. 699–712.
- Solum, J.G., van der Pluijm, B.A., and Peacor, D.R., 2005, Neocrystallization, fabrics and age of clay minerals from an exposure of the Moab fault, Utah: *Journal of Structural Geology*, v. 27, p. 1563–1576, doi:10.1016/j.jsg.2005.05.002.
- Spencer, J.E., 1996, Uplift of the Colorado Plateau due to lithospheric attenuation during Laramide low-angle subduction: *Journal of Geophysical Research*, v. 101, p. 13,595–13,609, doi:10.1029/96JB00818.

- Trudgill, B.D., 2011, Evolution of salt structures in the northern Paradox Basin: Controls on evaporite deposition, salt wall growth and supra-salt stratigraphic architecture: *Basin Research*, v. 23, no. 2, p. 208–238, doi:10.1111/j.1365-2117.2010.00478.x.
- van Wijk, J.W., Baldrige, W.S., van Hunen, J., Goes, S., Aster, R., Coblenz, D.D., Grand, S.P., and Ni, J., 2010, Small-scale convection at the edge of the Colorado Plateau: Implications for topography, magmatism, and evolution of Proterozoic lithosphere: *Geology*, v. 38, p. 611–614, doi:10.1130/G31031.1.
- Weber, K.A., Spanbauer, T.L., Wacey, D., Kilburn, M.R., Loope, D.B., and Kettler, R.M., 2012, Biosignatures link microorganisms to iron mineralization in a paleoquifer: *Geology*, v. 40, p. 747–750, doi:10.1130/G33062.1.
- Wernicke, B., 2011, The California River and its role in carving Grand Canyon: *Geological Society of America Bulletin*, v. 123, p. 1288–1316, doi:10.1130/B30274.1.
- Whipp, D.M., and Ehlers, T.A., 2007, Influence of groundwater flow on thermochronometer-derived exhumation rates in the central Nepalese Himalaya: *Geology*, v. 35, p. 851–854, doi:10.1130/G23788A.1.
- Wigley, M., Kampman, N., Dubacq, B., and Mickle, M., 2012, Fluid-mineral reactions and trace metal mobilization in an exhumed natural CO₂ reservoir, Green River, Utah: *Geology*, v. 40, p. 555–558, doi:10.1130/G32946.1.
- Winkler, D.A., Jacobs, L.L., Congleton, J.D., and Downs, W.R., 1991, Life in a sand sea: Biota from Jurassic interdunes: *Geology*, v. 19, p. 889–892, doi:10.1130/0091-7613(1991)019<0889:LIASSB>2.3.CO;2.
- Wong, I.G., and Humphrey, J.R., 1989, Contemporary seismicity, faulting, and the state of stress in the Colorado Plateau: *Geological Society of America Bulletin*, v. 101, p. 1127–1146, doi:10.1130/0016-7606(1989)101<1127:CSFATS>2.3.CO;2.
- Worster, D., 2002, *A River Running West: The Life of John Wesley Powell*: Oxford, UK, Oxford University Press, 688 p.

MANUSCRIPT ACCEPTED BY THE SOCIETY 9 JUNE 2016

